Supplementary Material

Observed Evidence of Frequency-Dependent Site Amplification Due to Structural Control of Active Reverse Faults at Different Localities in Japan

TABLE OF CONTENTS:

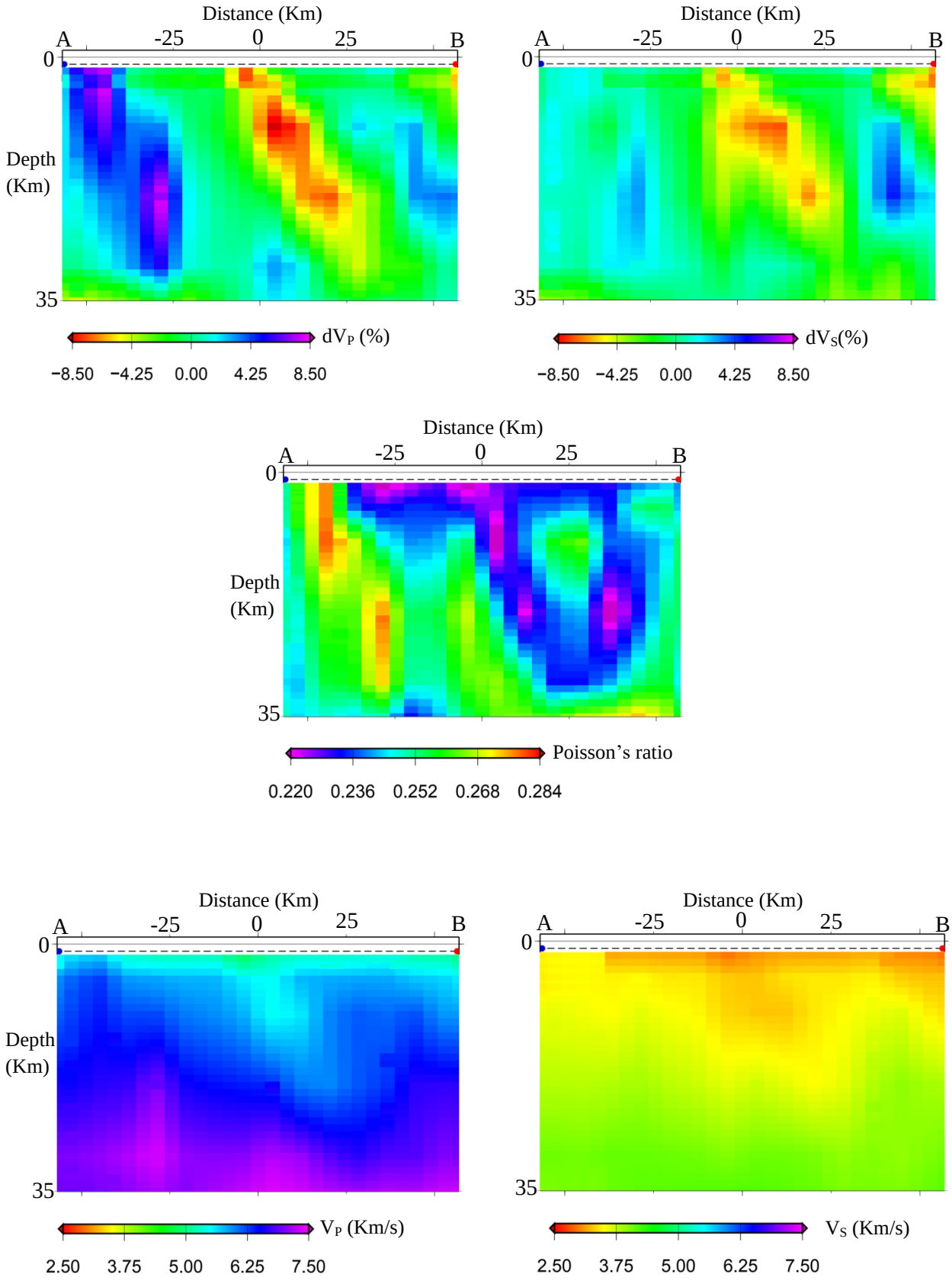

Figure S1: Subsurface tomography structures along profile AB in East Hokkaido study area.

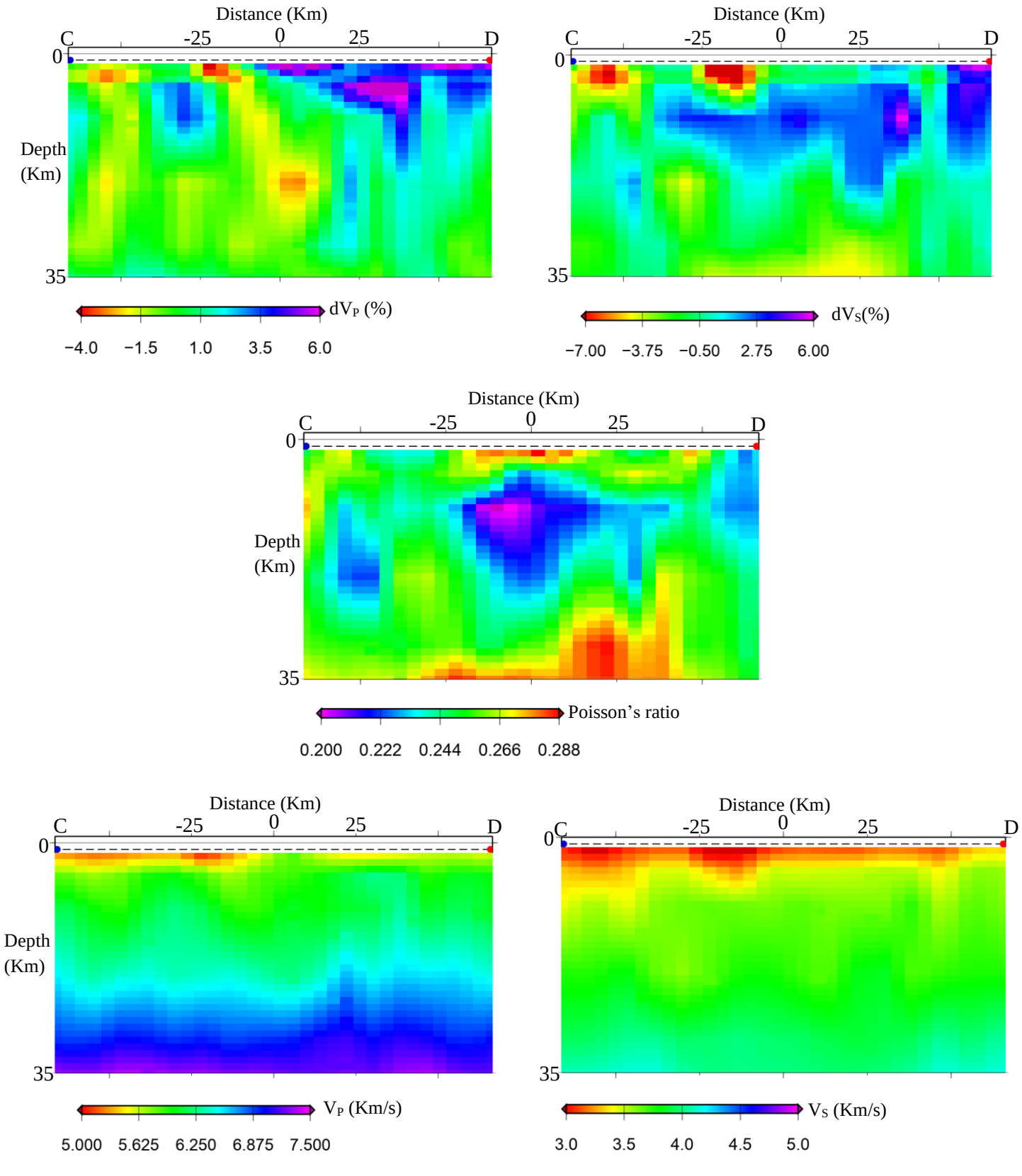

Figure S2: Subsurface tomography structures along profile CD in Akita-Iwate study area.

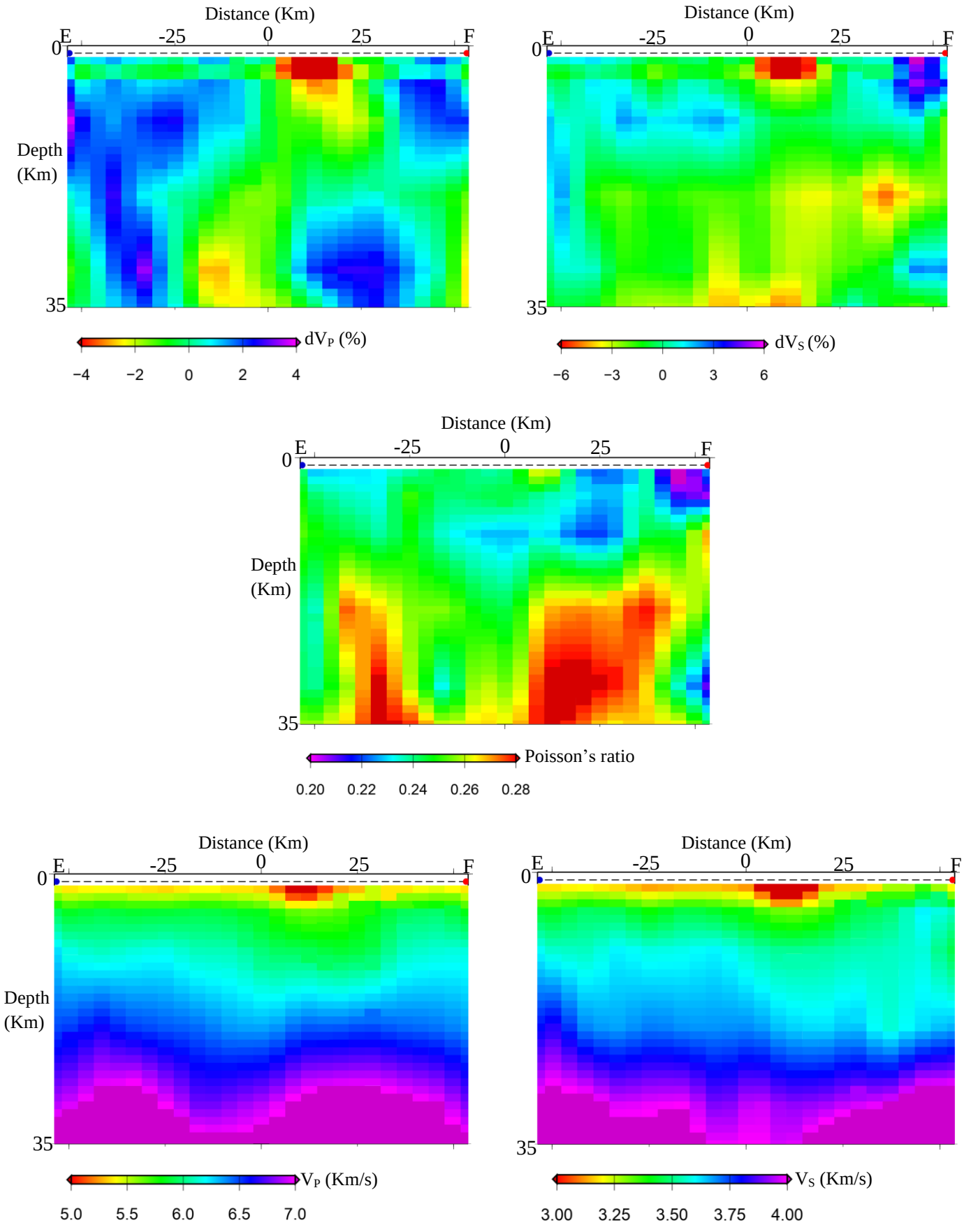

Figure S3: Subsurface tomography structures along profile EF in Akita-Iwate study area.

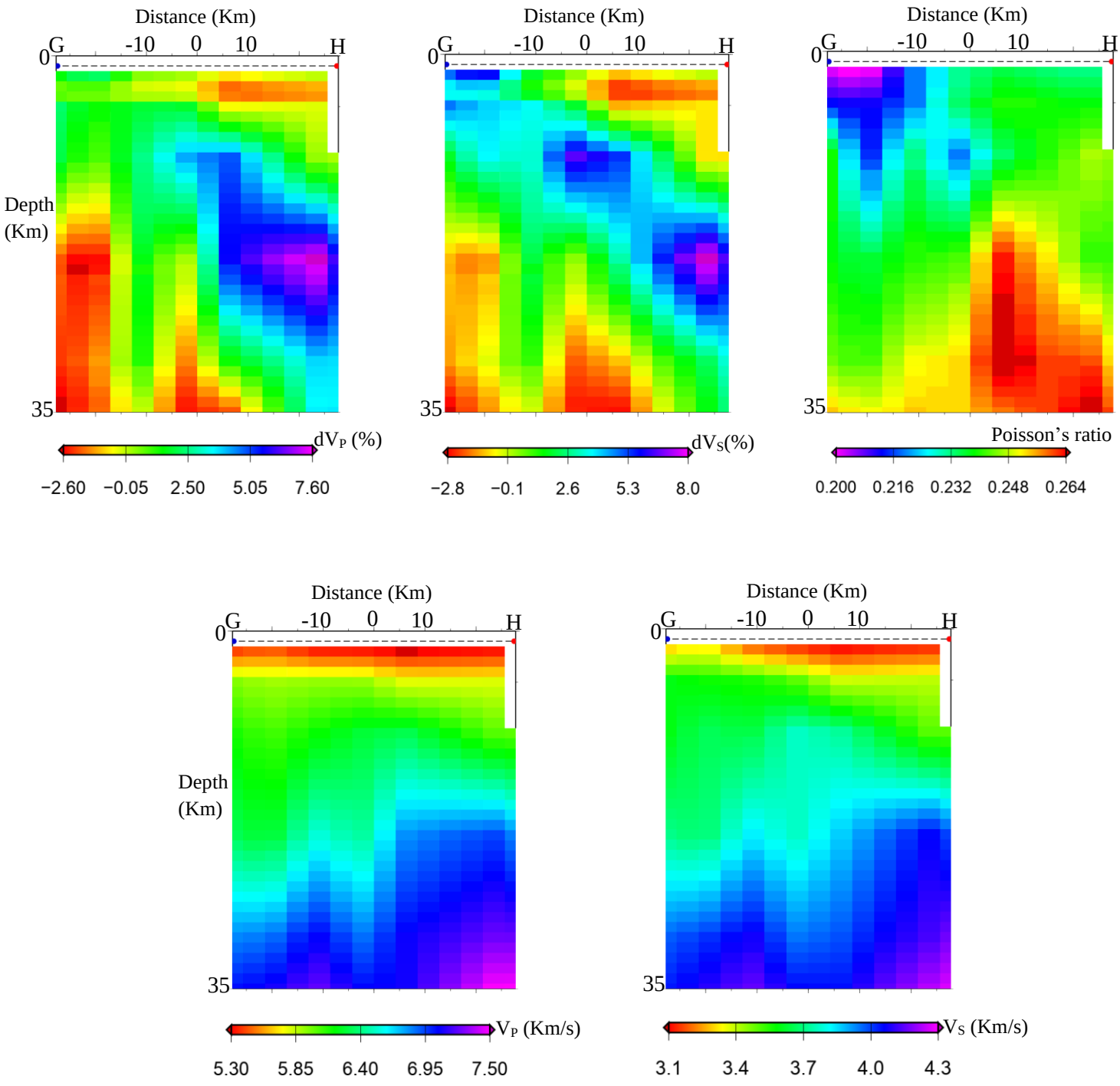

Figure S4: Subsurface tomography structures along profile GH in Fukushima study area based on calculation by Nakamura *et al*. (2008).

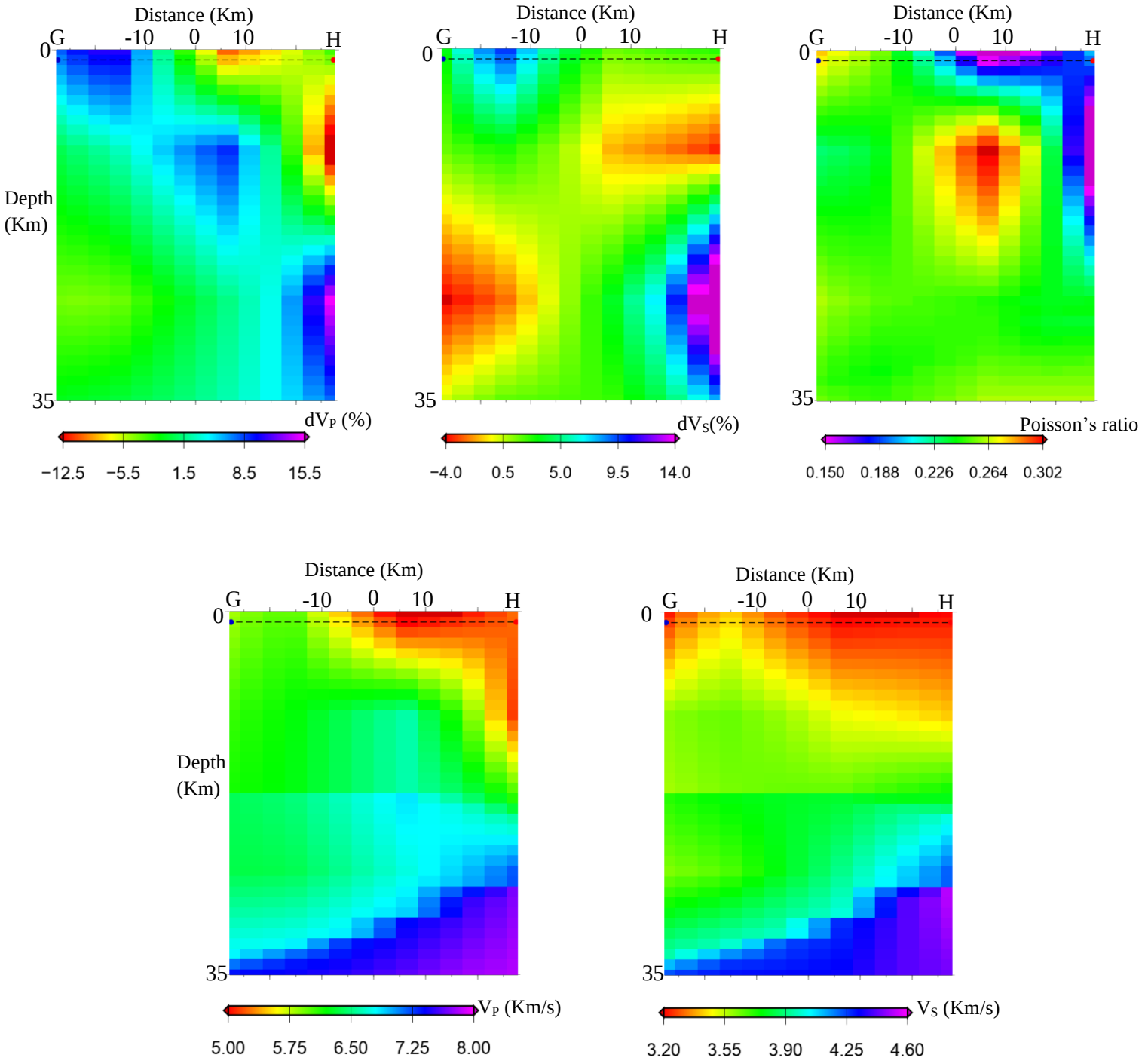

Figure S5: Subsurface tomography structures along profile GH in Fukushima study area based on calculation by Nakajima *et al*. (2001).

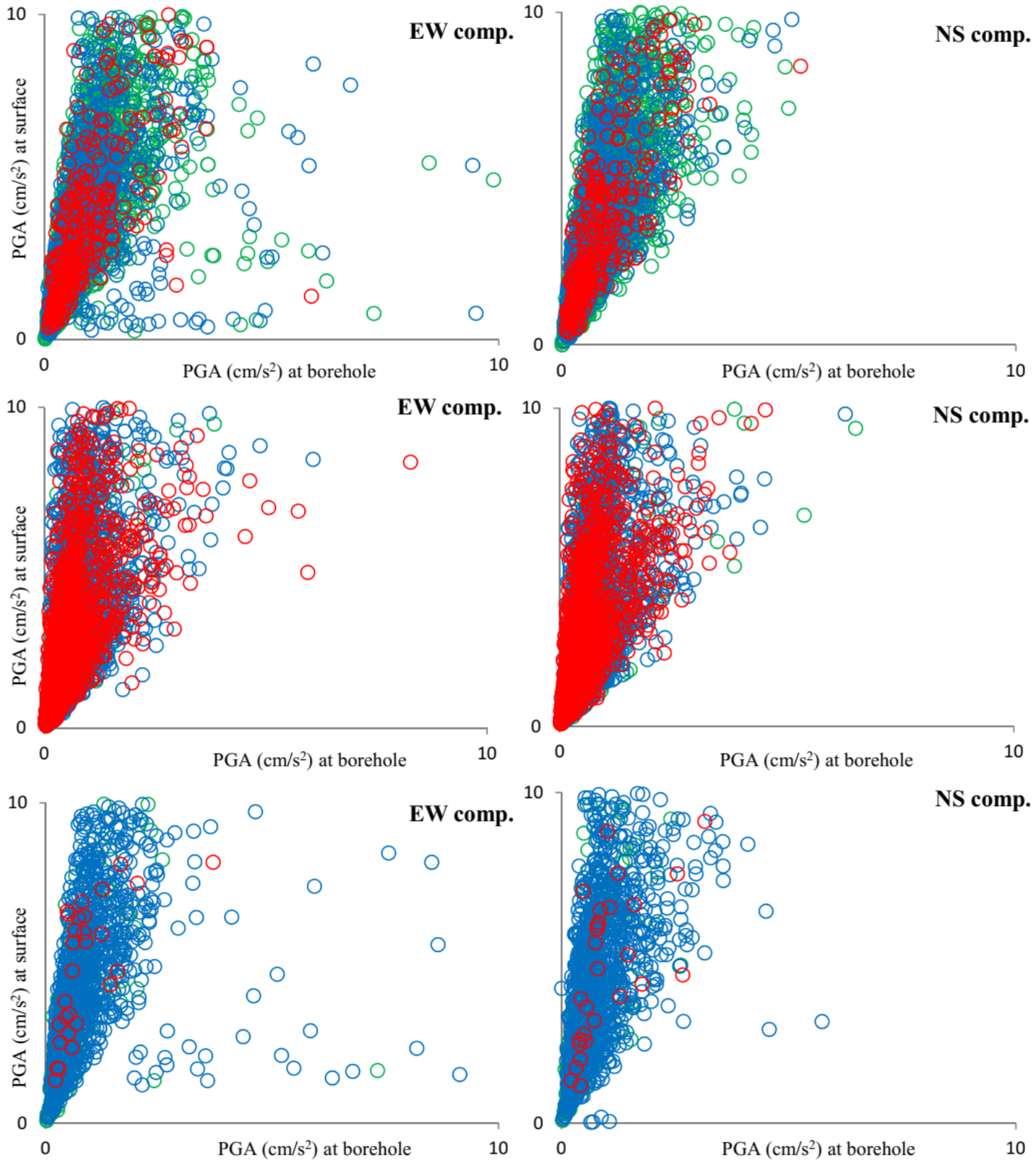

Figure S6: Correlation between PGAs of EW and NS components at surface and borehole obtained from KiK-net stations at the East Hokkaido (upper), Akita-Iwate (middle), and Fukushima (lower) study areas. (Note: colors of green, blue, and red are used to discriminate PGAs on HW (l.FW in the Akita-Iwate study area), FW (r.FW in Akita-Iwate study area), and FZ (upthrown blocks in the Akita-Iwate study area), respectively)

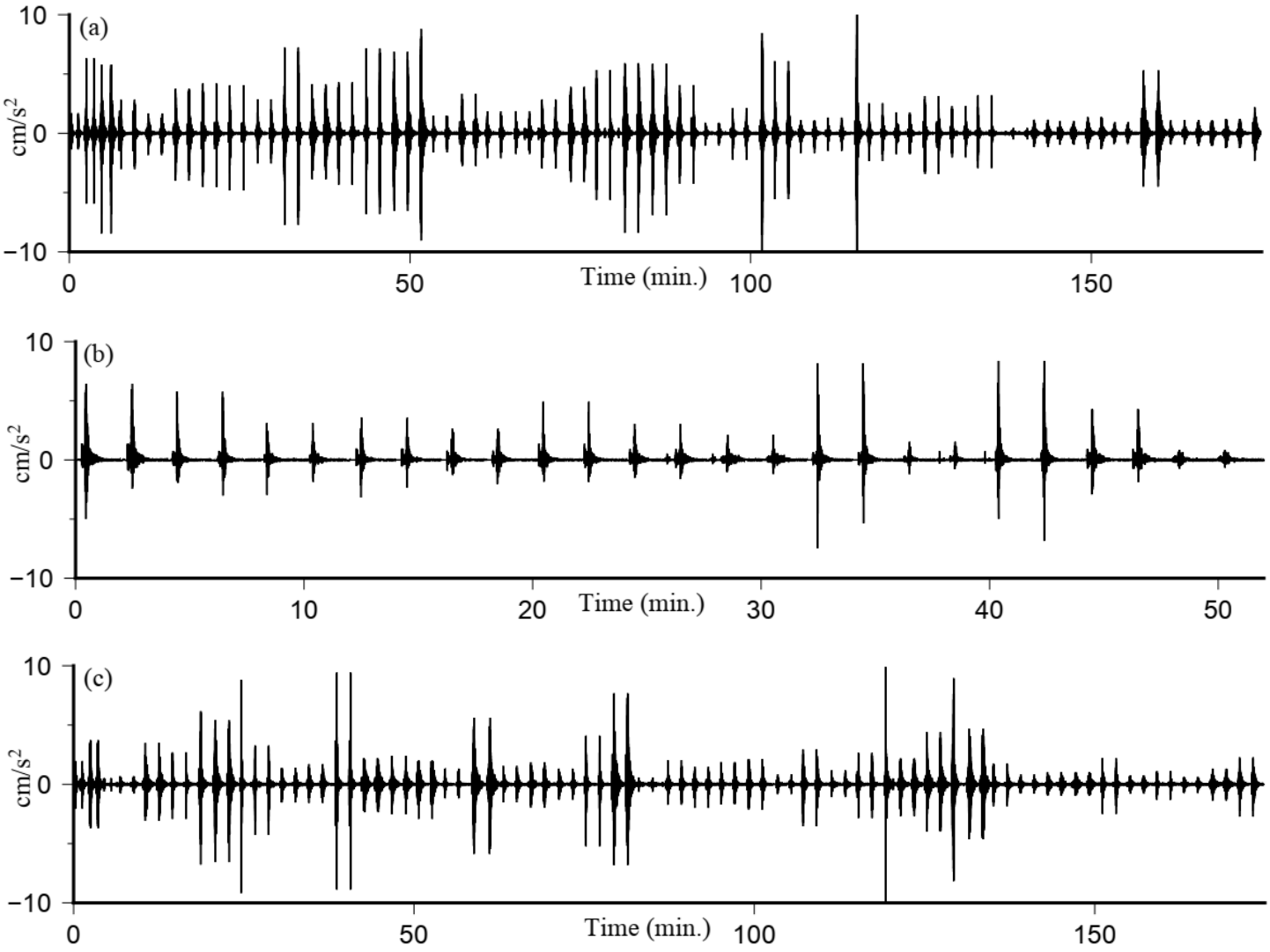

Figure S7: Example of continuous time series of EW components recorded at TKCH05 KiK-net station with their hypocenters located beneath FW (a), FZ (b), HW (c).

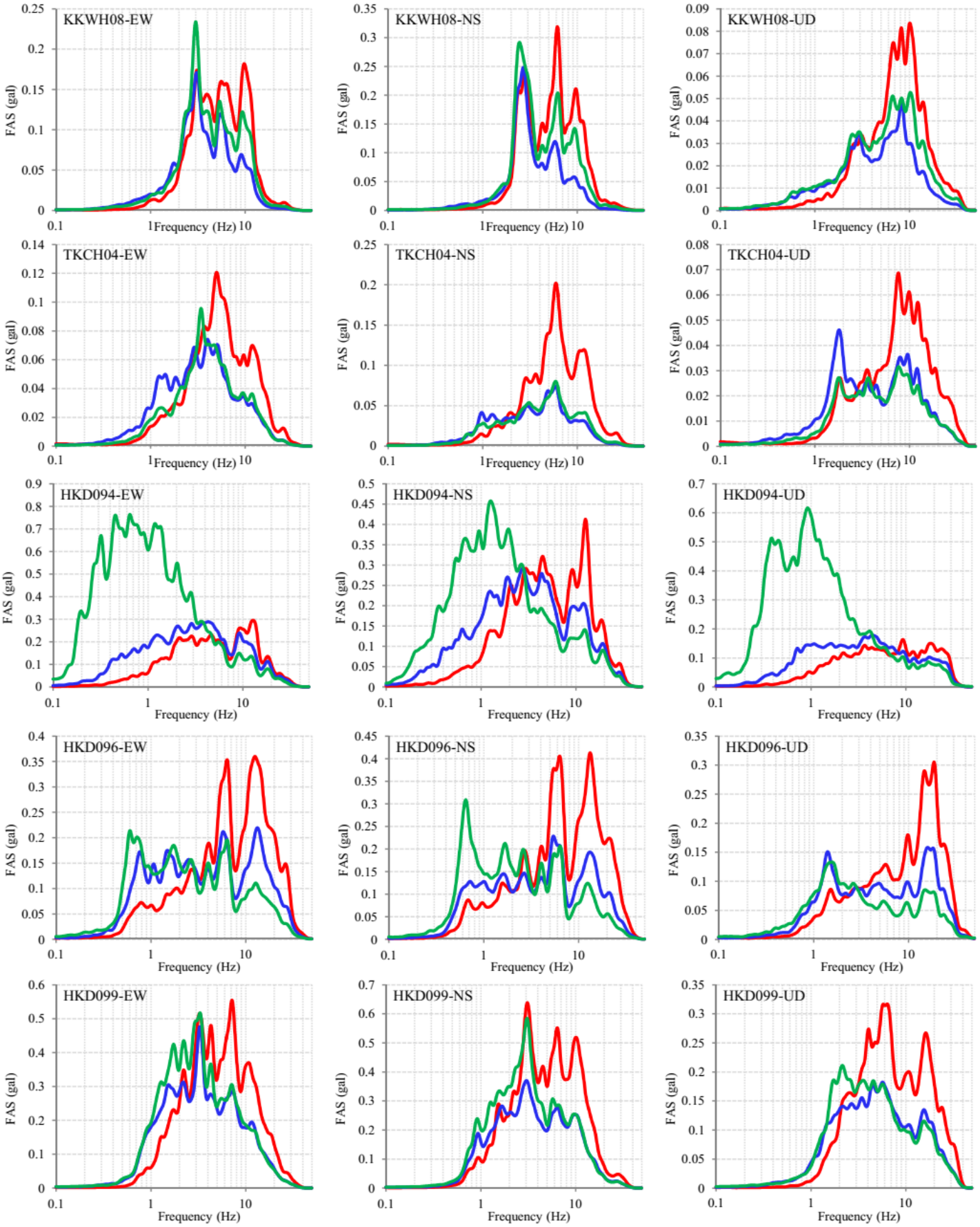

Figure S8: FASs at seismic stations located on FW block in the East Hokkaido study area due to recorded EFWs (blue), EFZs (red), and EHWs (green).

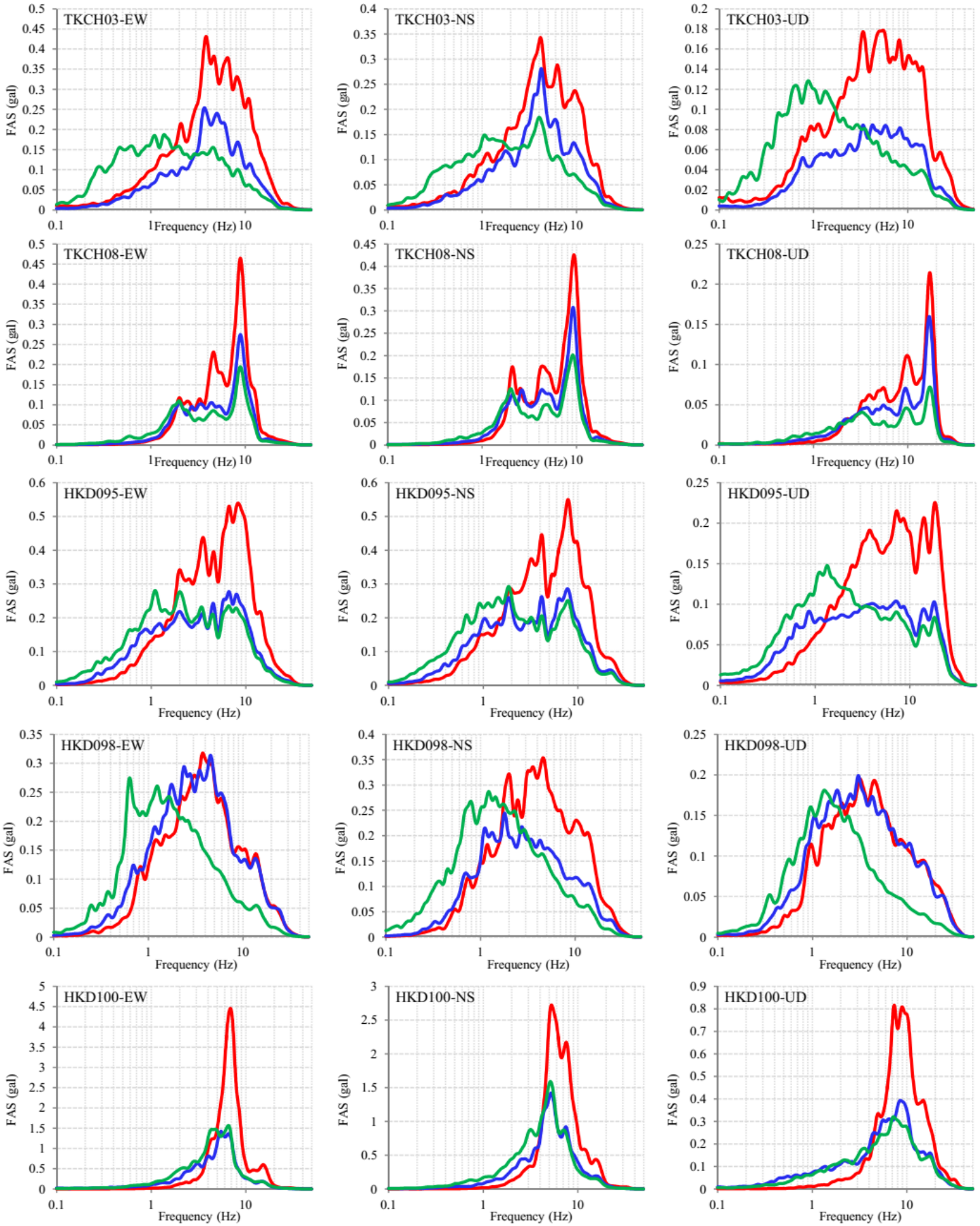

Figure S9: FASs at seismic stations located on FZ in the East Hokkaido study area due to recorded EFWs (blue), EFZs (red), and EHWs (green).

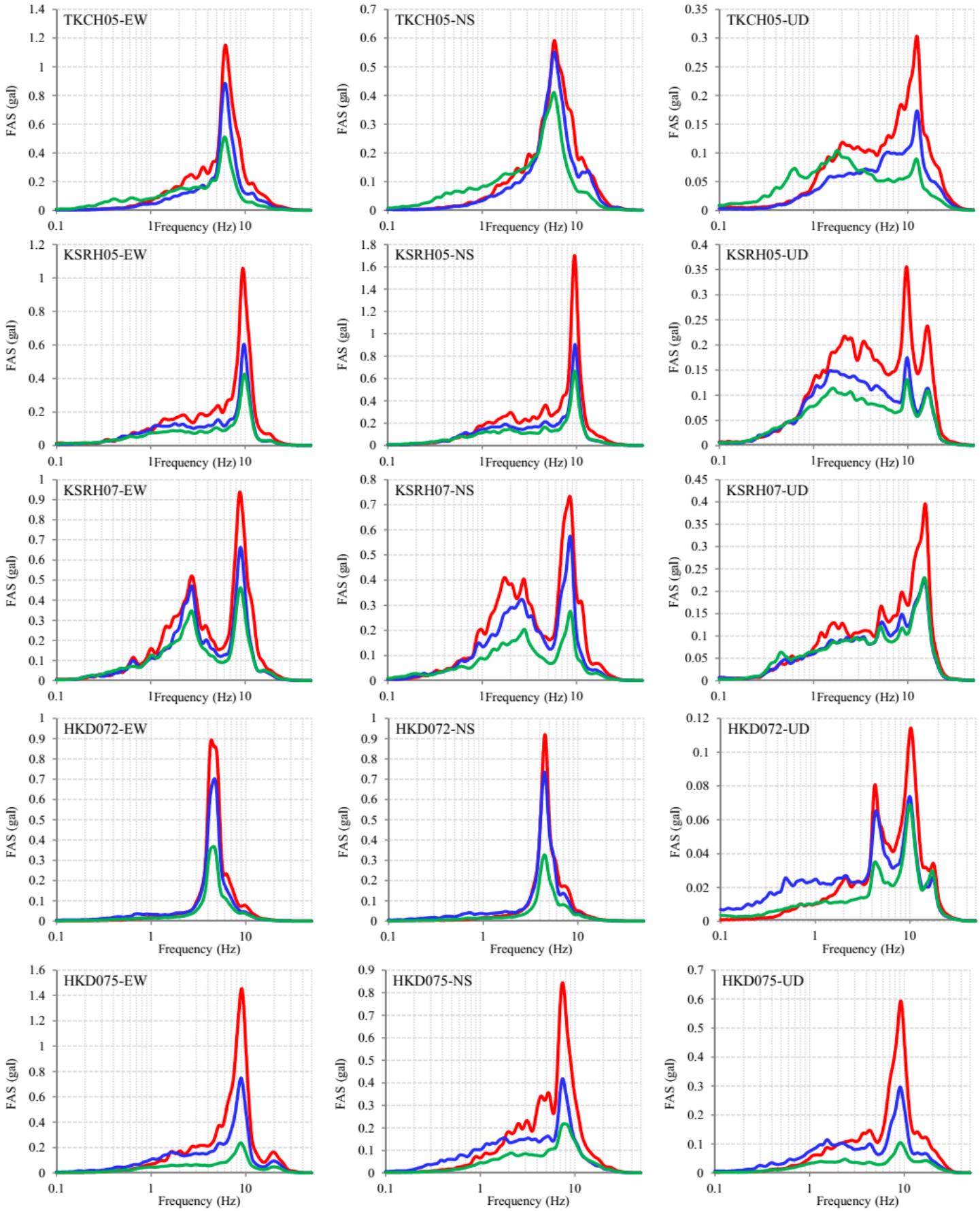

Figure S10: FASs at seismic stations located on HW block in the East Hokkaido study area due to recorded EFWs (blue), EFZs (red), and EHWs (green).

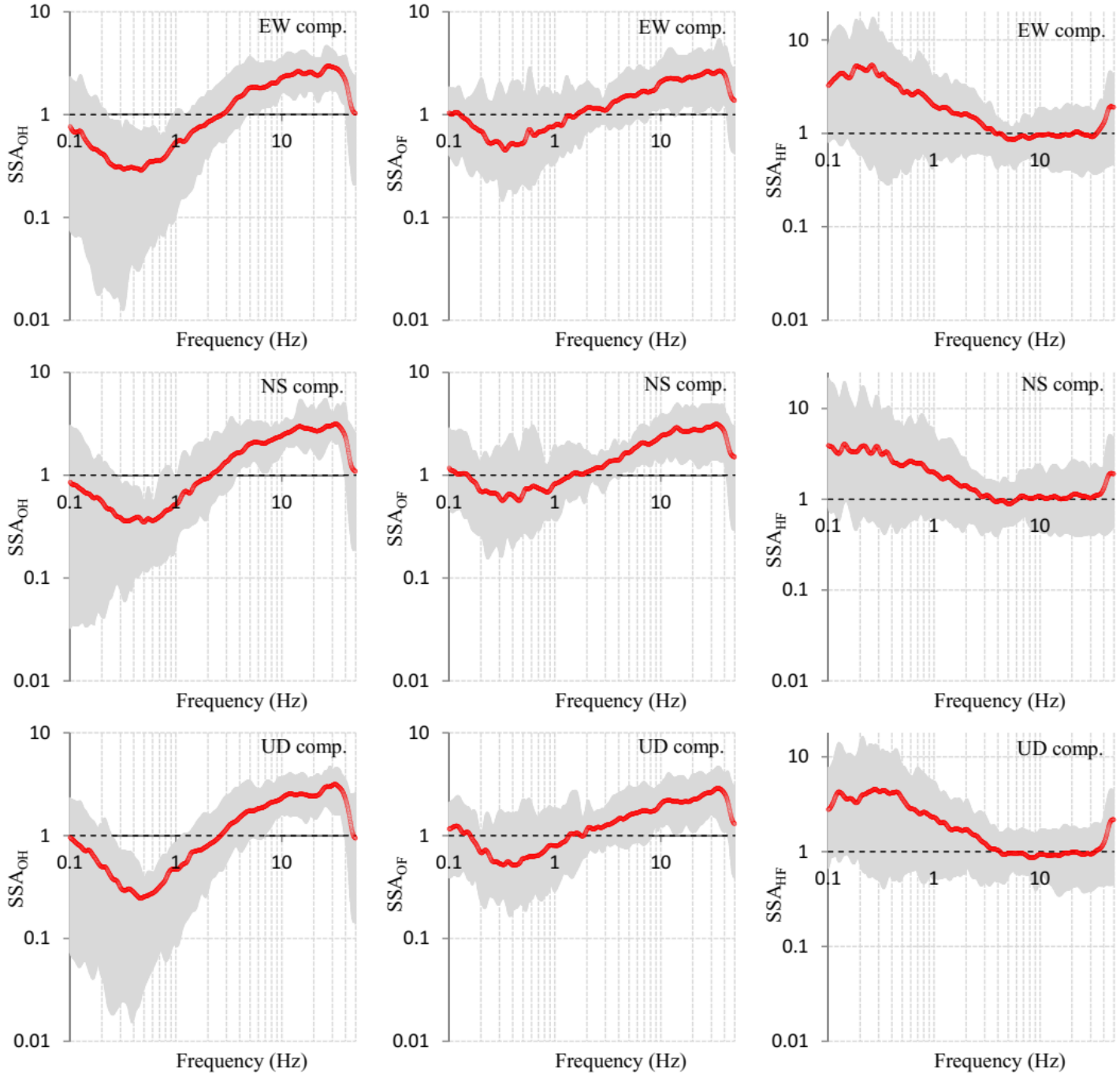

Figure S11: The estimated average SSAs (red) with their minimum and maximum (gray), which are calculated based on equations 1, 2, and 3 for the seismic stations located on the FW block in East Hokkaido study area.

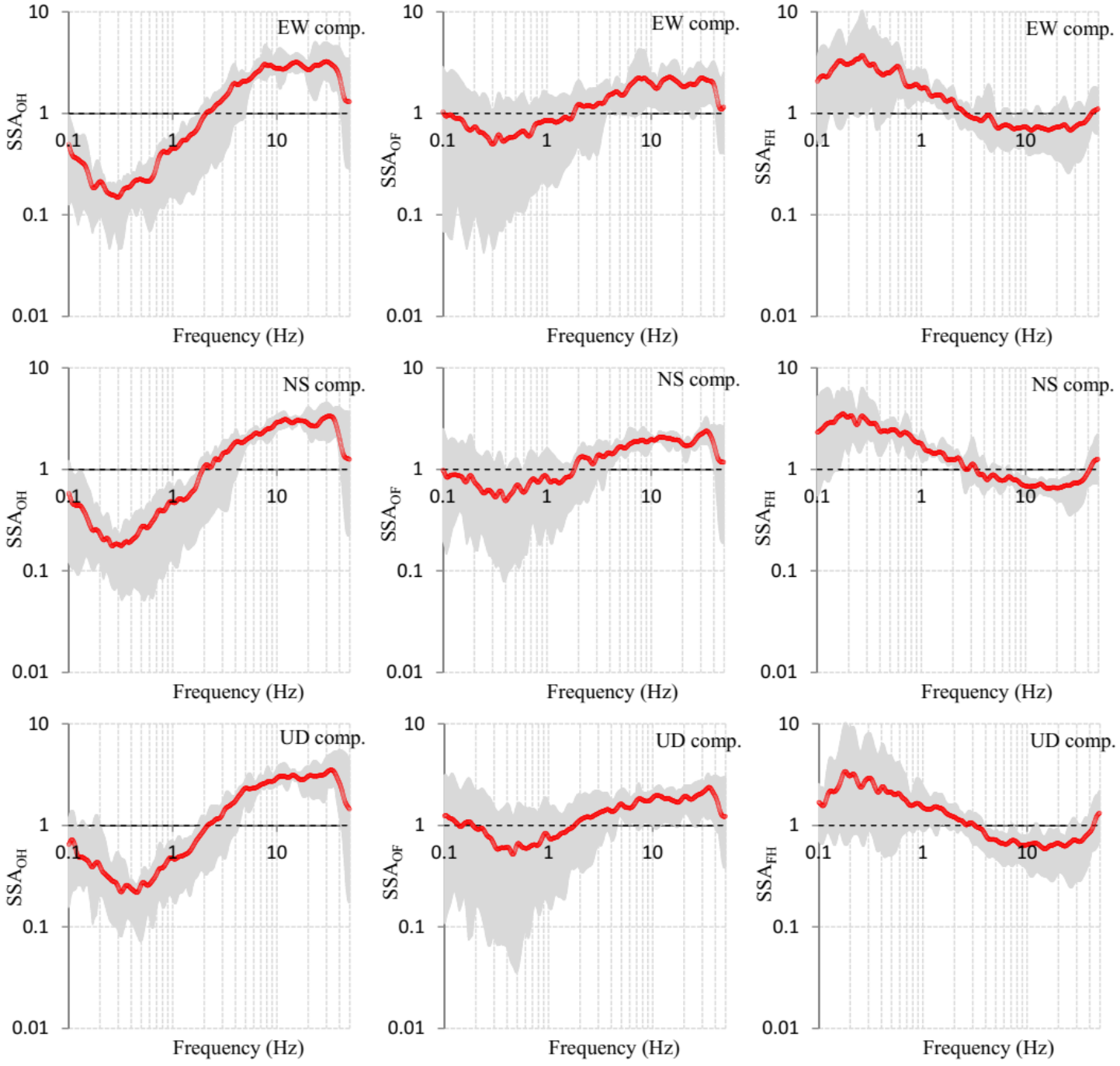

Figure S12: The estimated average SSAs (red) with their minimum and maximum (gray), which are calculated based on equations 1, 2, and 4 for the seismic stations located on the FZ in East Hokkaido study area.

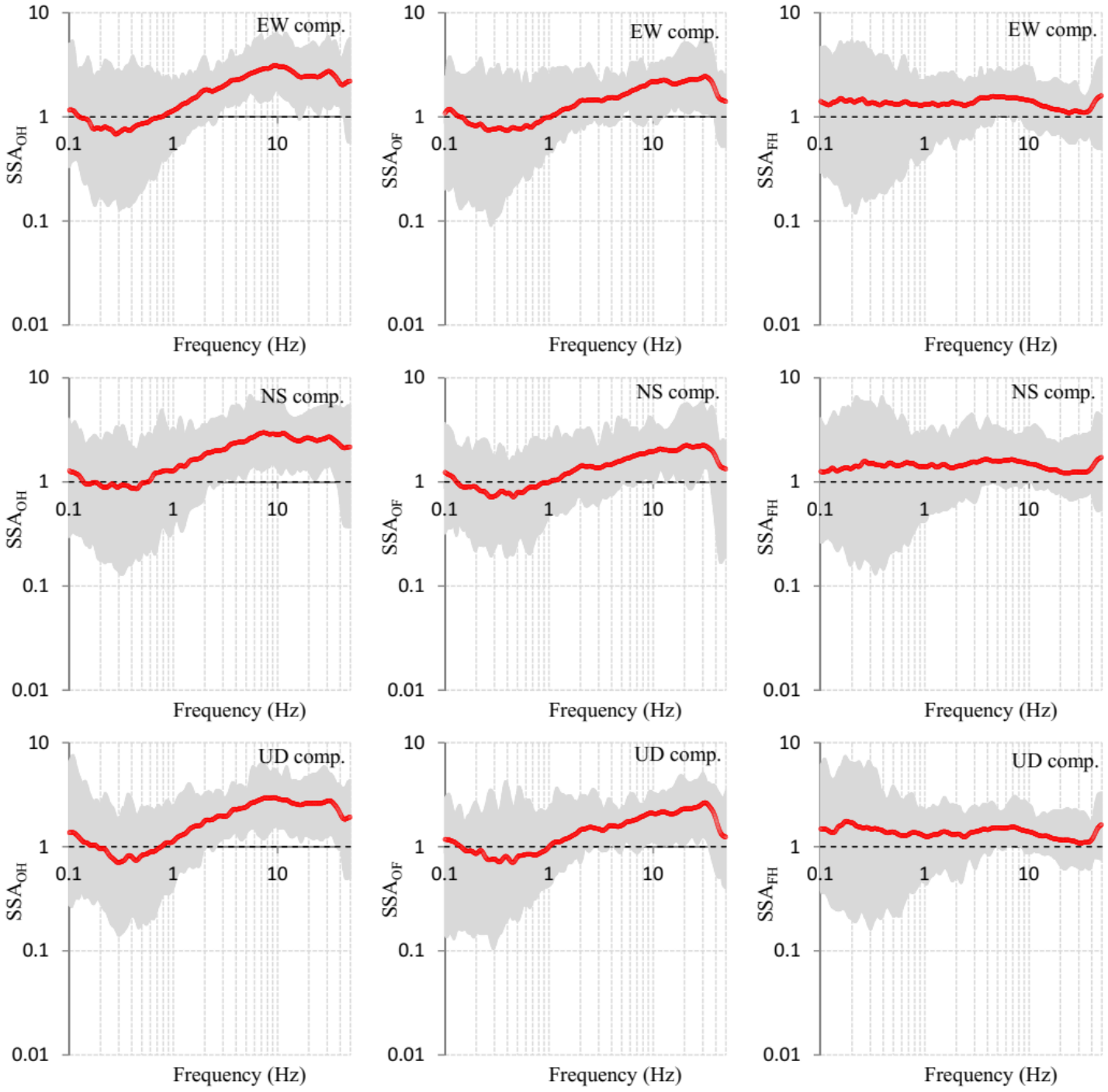

Figure S13: The estimated average SSAs (red) with their minimum and maximum (gray), which are calculated based on equations 1, 2, and 4 for the seismic stations located on the HW block in East Hokkaido study area.

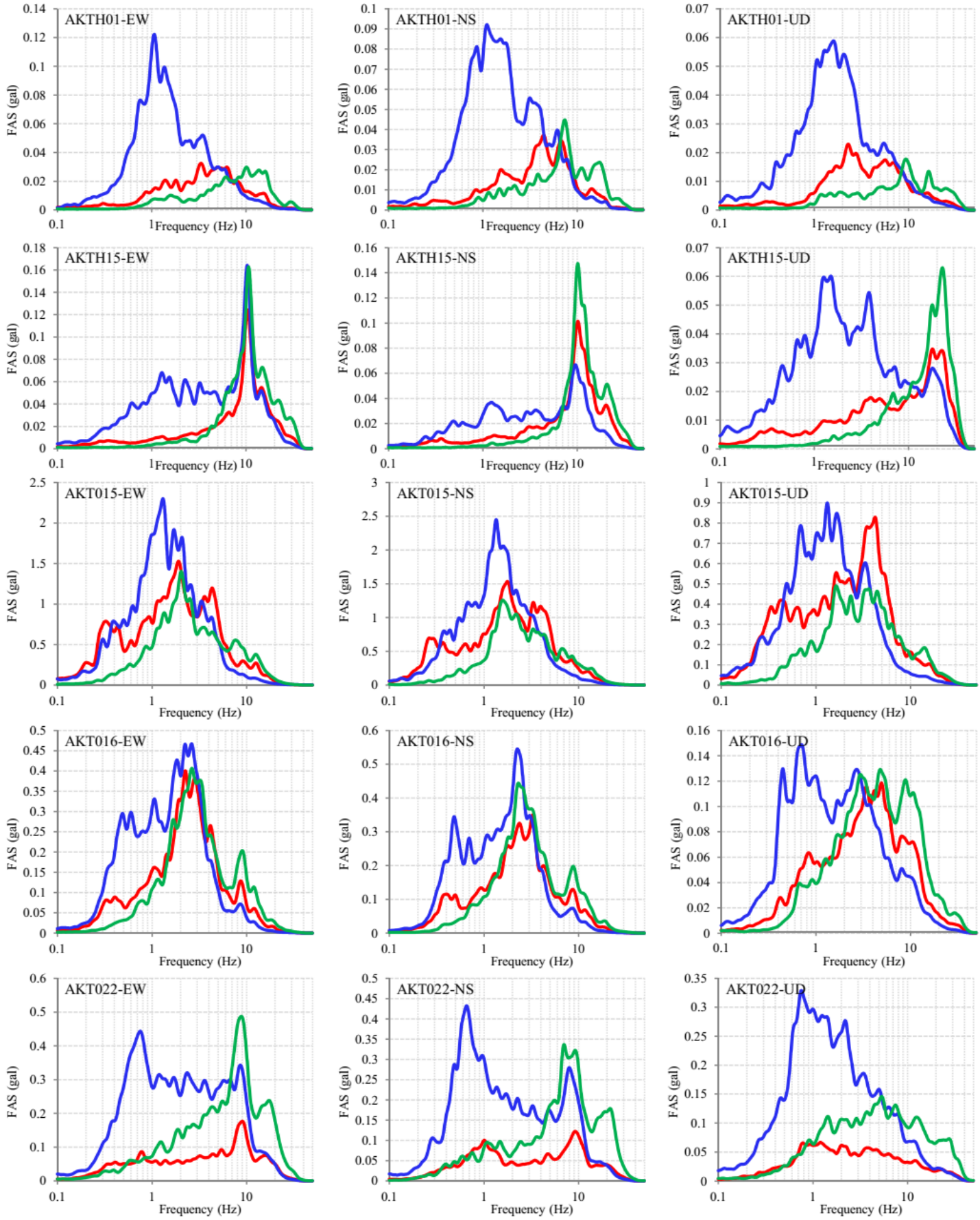

Figure S14: FASs at seismic stations located on l.FW block in Akita-Iwate study area due to recorded El.FWs (green), EFZs (red), and Er.FWs (blue).

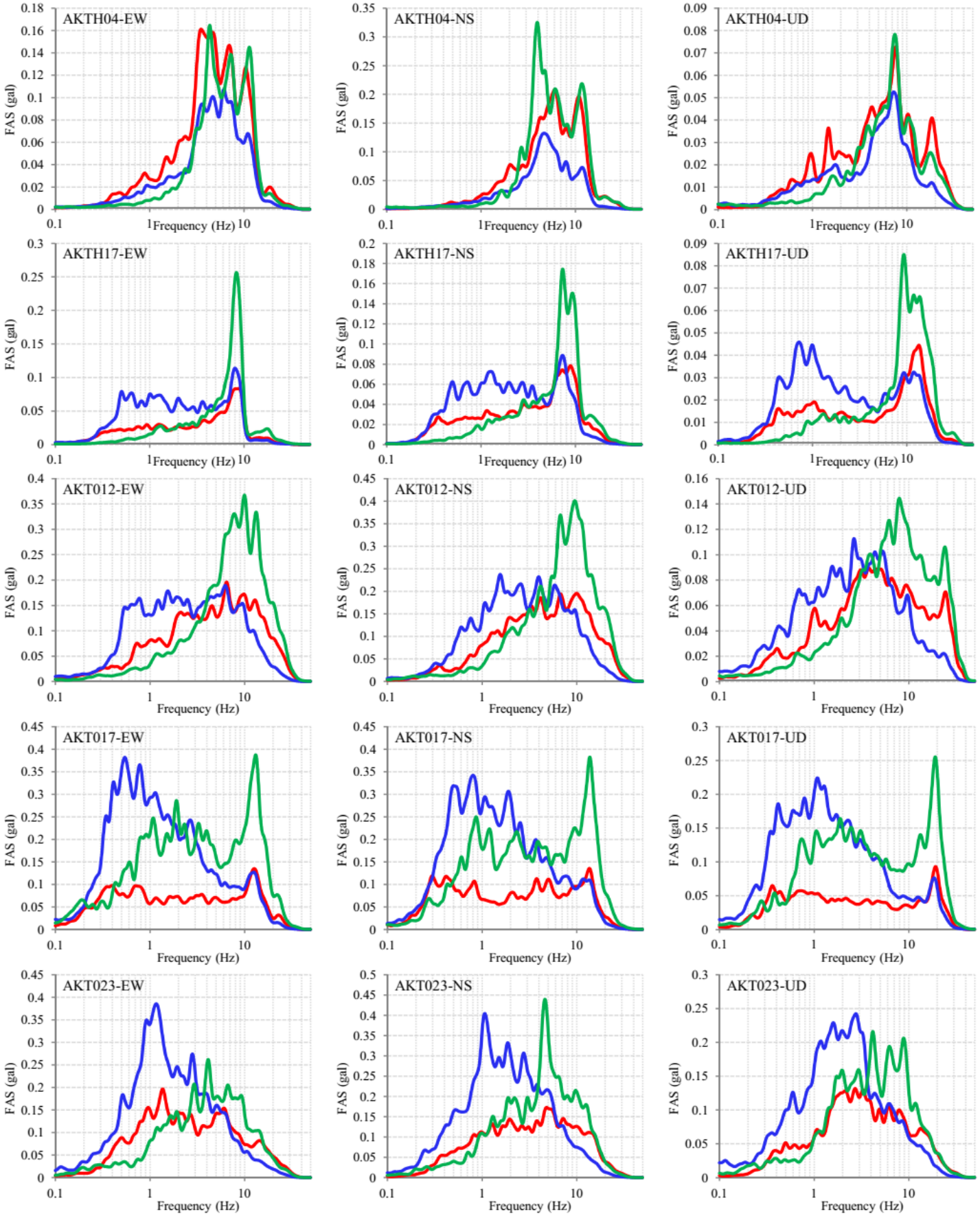

Figure S15: FASs at seismic stations located on FZ in Akita-Iwate study area due to recorded El.FWs (green), EFZs (red), and Er.FWs (blue).

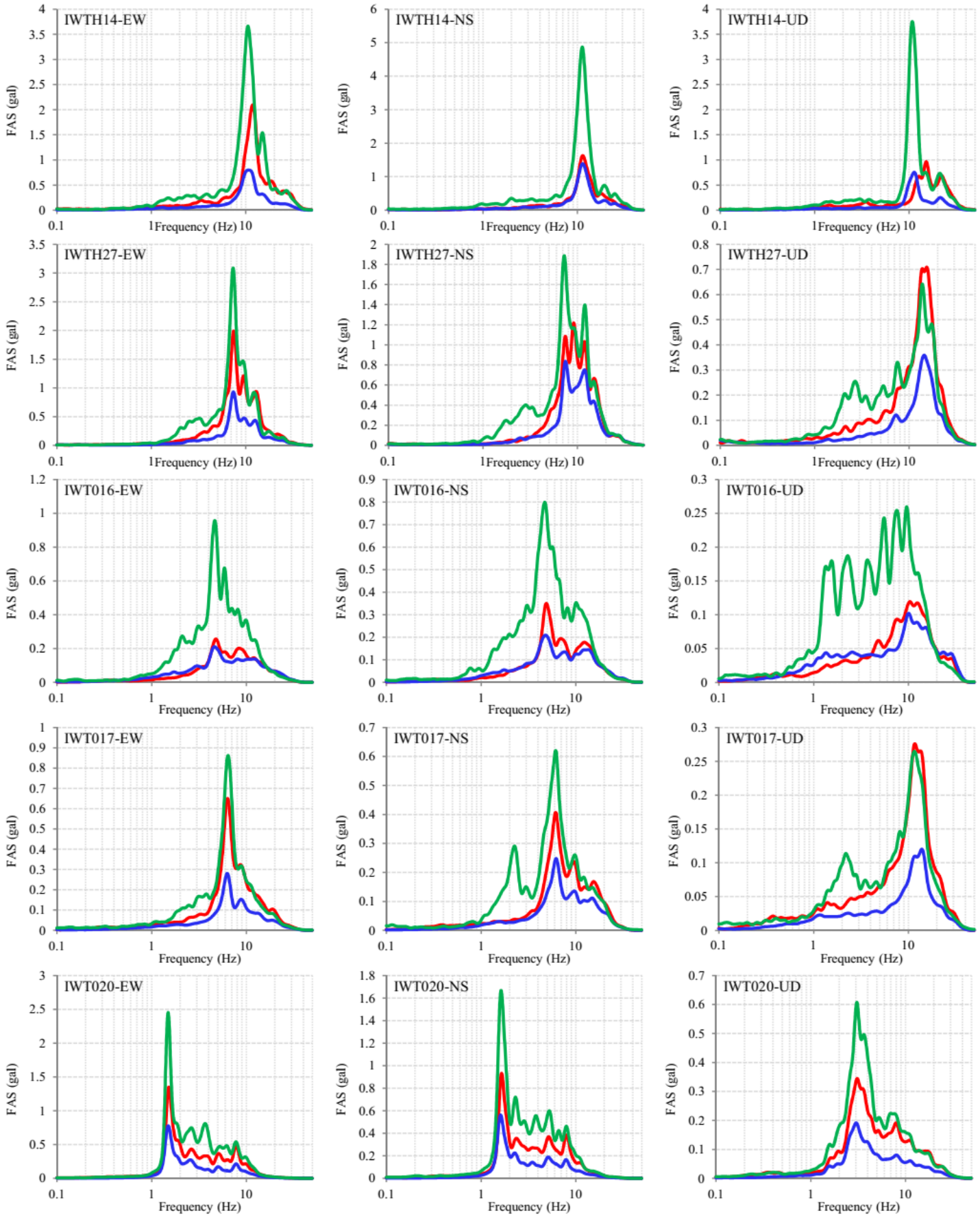

Figure S16: FASs at seismic stations located on r.FW block in Akita-Iwate study area due to recorded El.FWs (green), EFZs (red), and Er.FWs (blue).

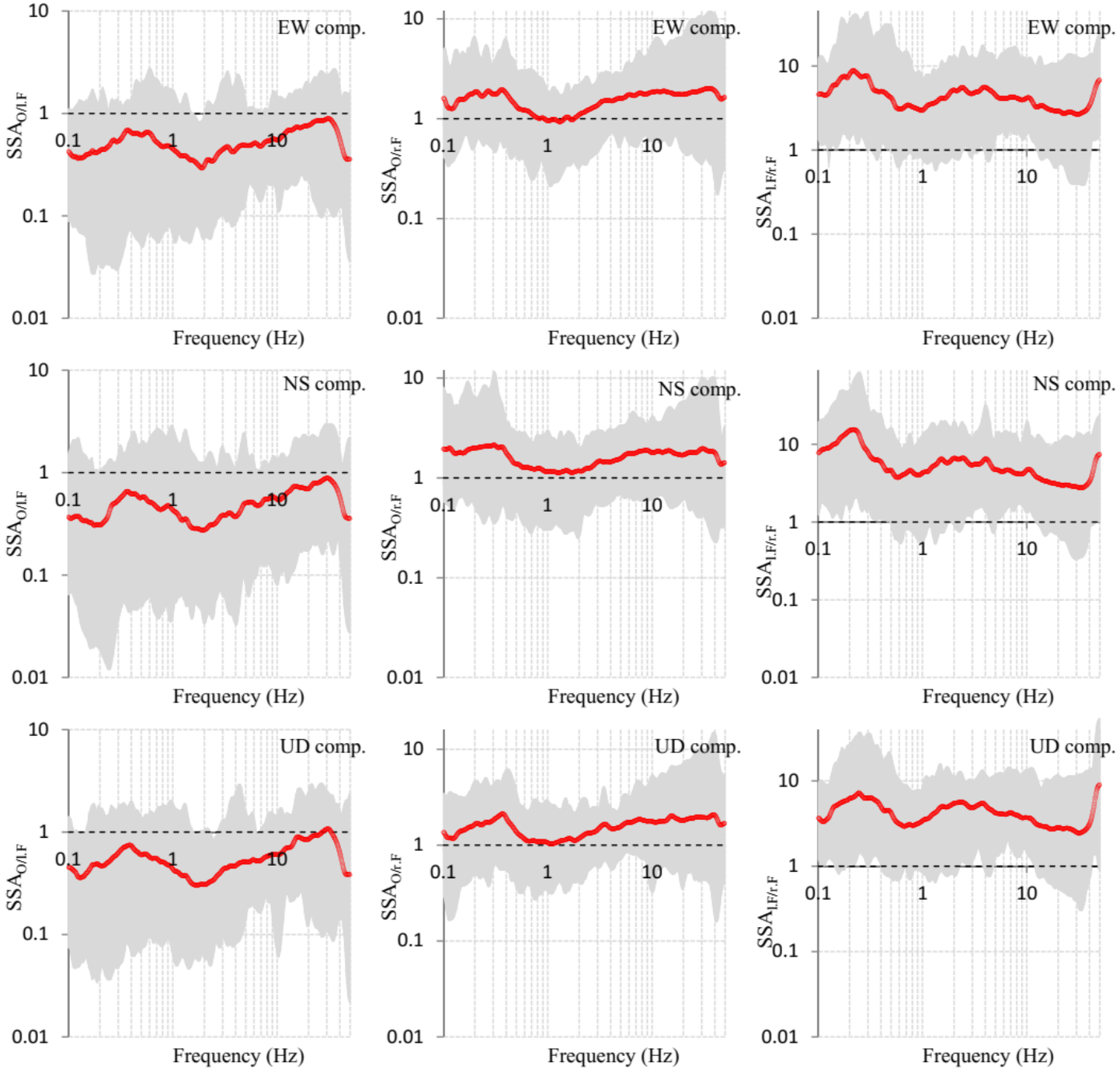

Figure S17: The estimated average SSAs (red) with their minimum and maximum (gray), which are calculated based on equations 1, 2, and 3 for the seismic stations located on the r.FW block in Akita-Iwate study area.

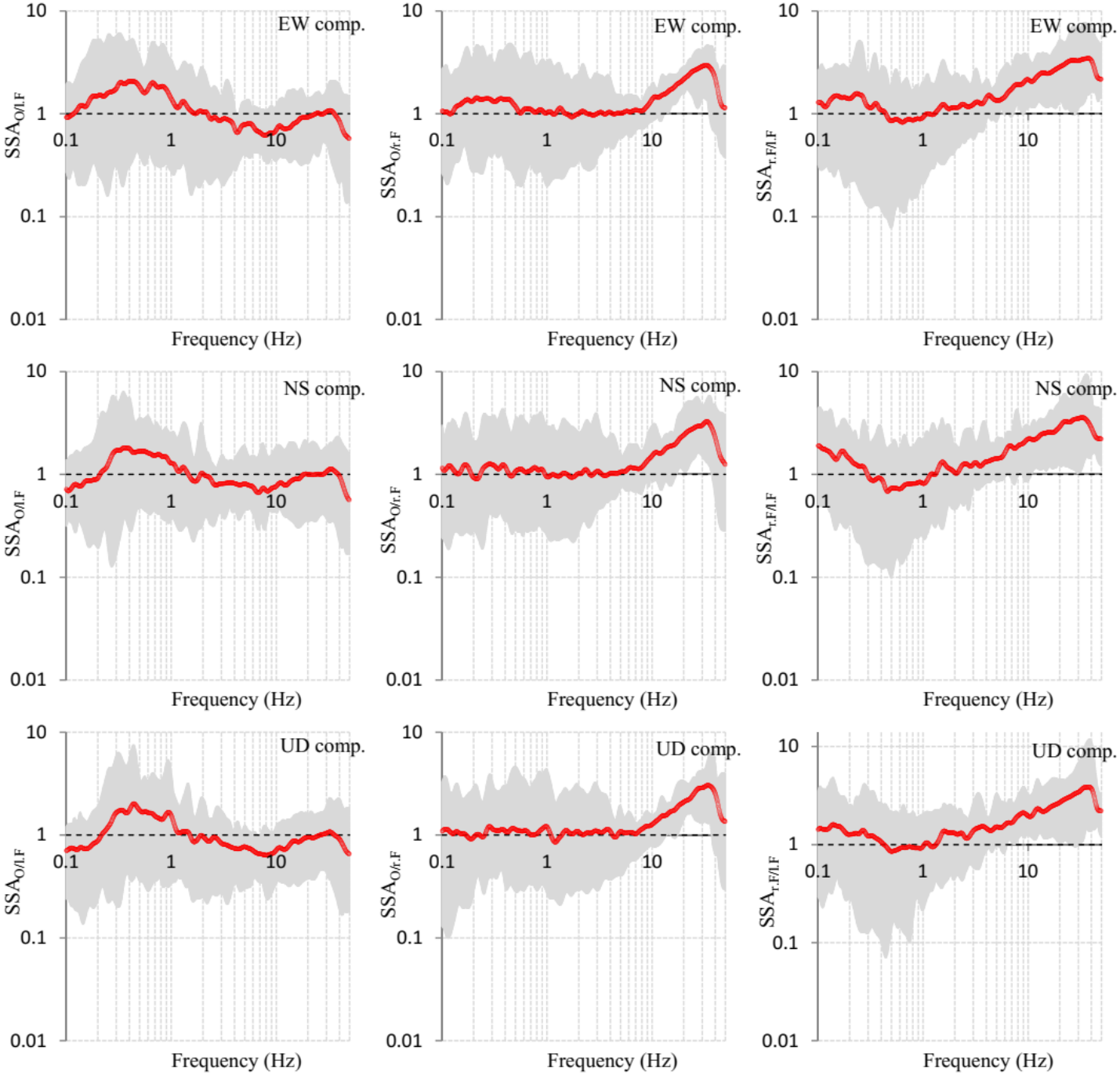

Figure S18: The estimated average SSAs (red) with their minimum and maximum (gray), which are calculated based on equations 1, 2, and 4 for the seismic stations located on the FZ in Akita-Iwate study area.

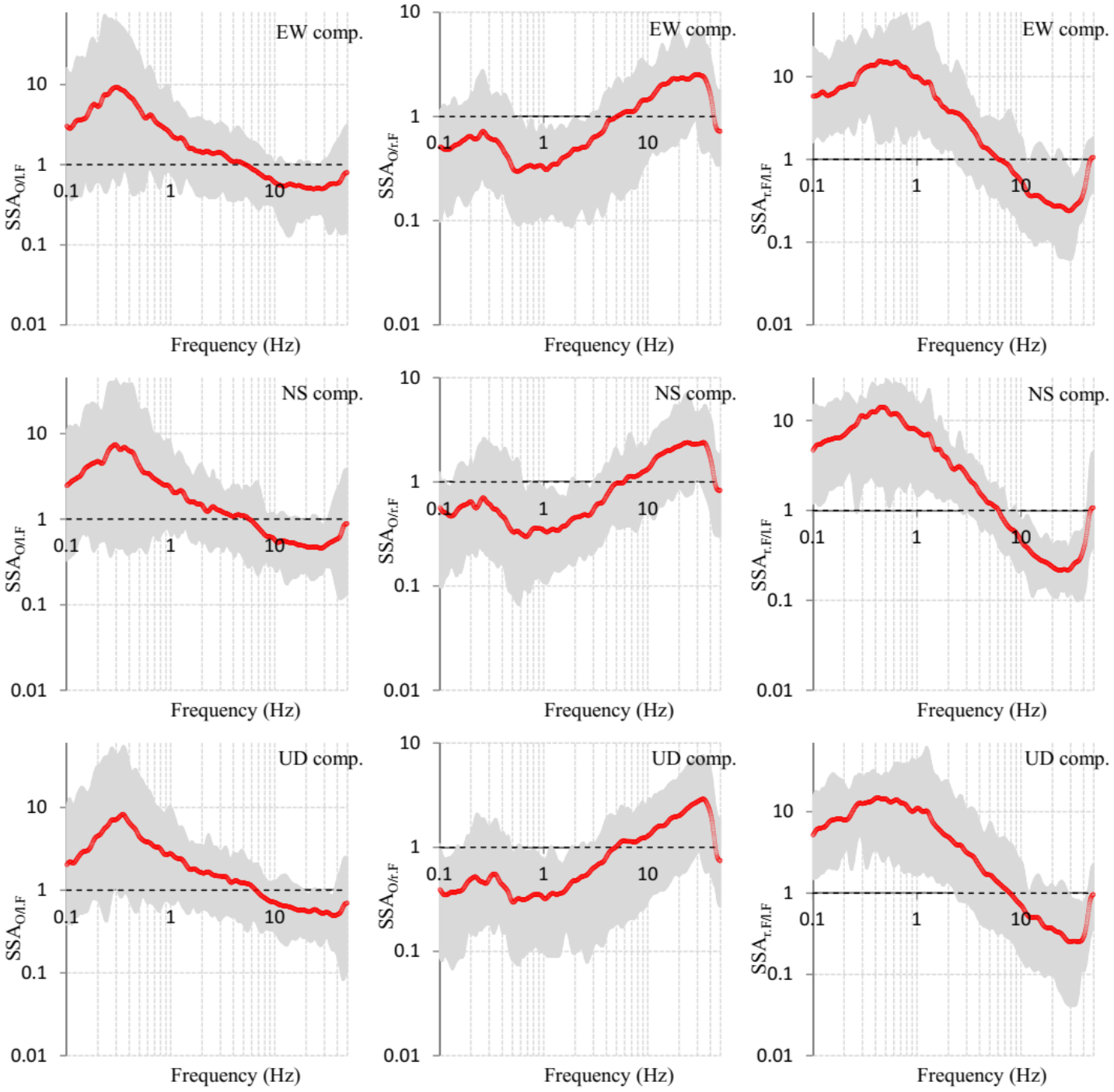

Figure S19: The estimated average SSAs (red) with their minimum and maximum (gray), which are calculated based on equations 1, 2, and 4 for the seismic stations located on the l.FW block in Akita-Iwate study area.

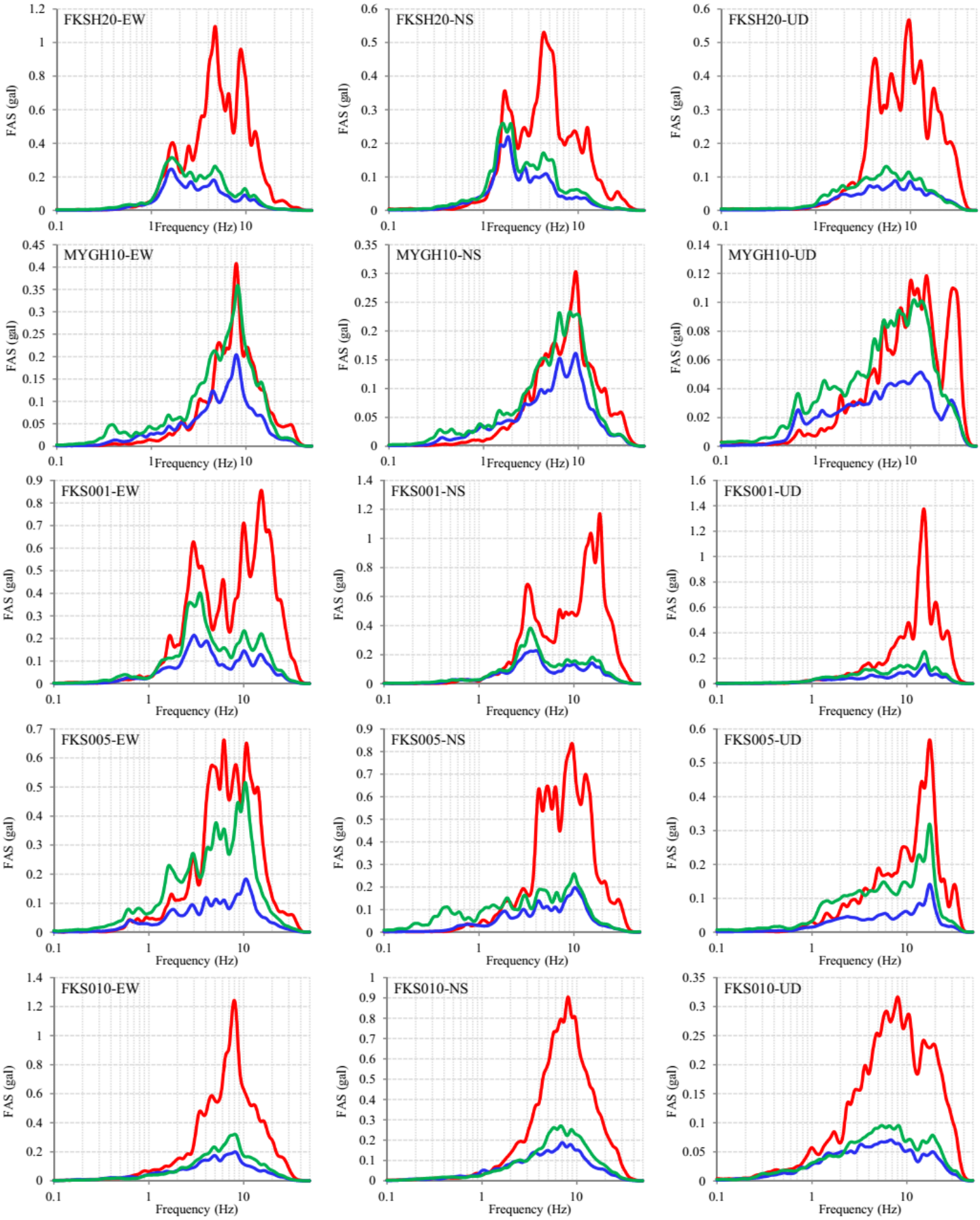

Figure S20: FASs at seismic stations located on FW block in Fukushima study area due to recorded EFWs (blue), EFZs (red), and EHWs (green).

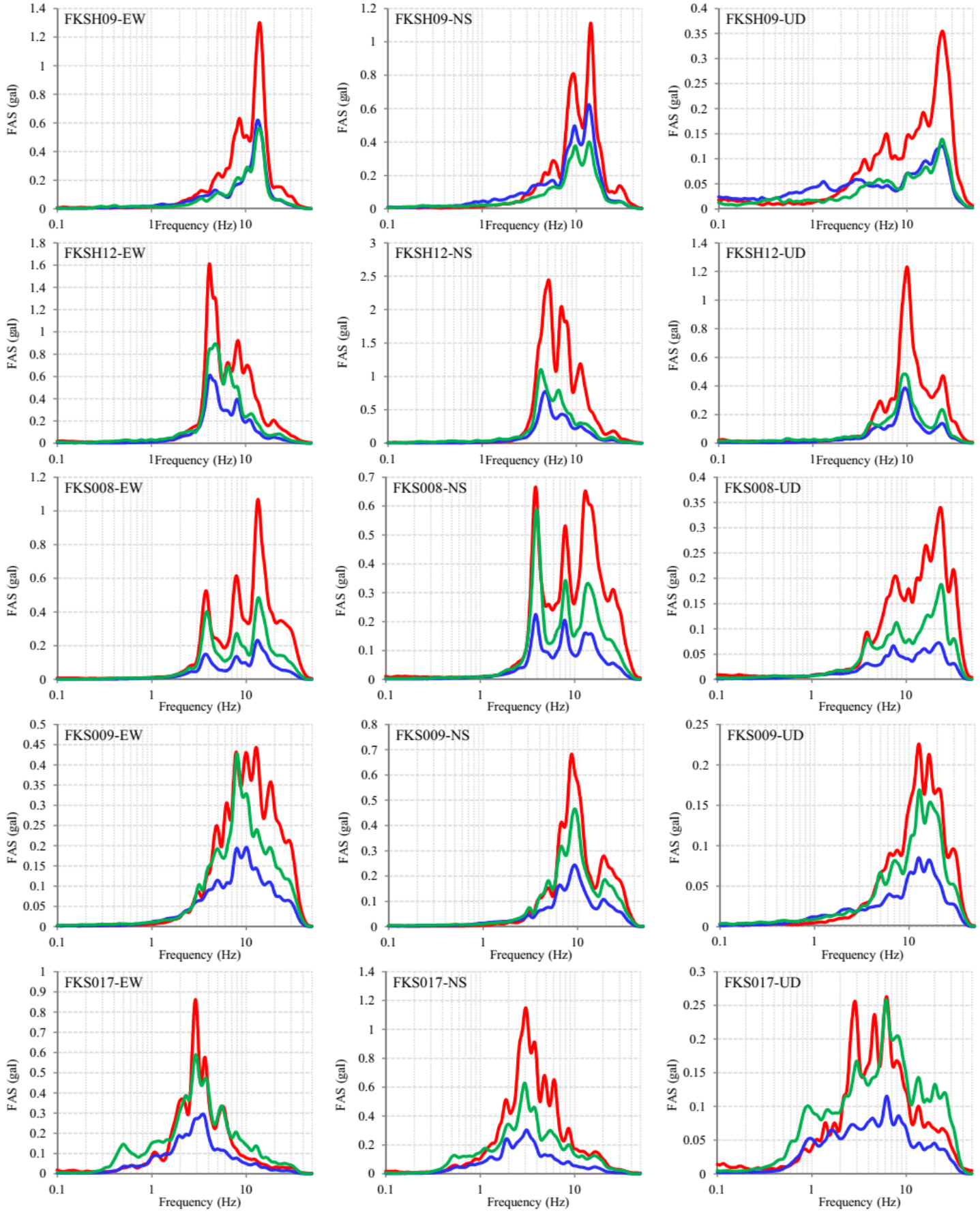

Figure S21: FASs at seismic stations located on HW block in Fukushima study area due to recorded EFWs (blue), EFZs (red), and EHWs (green).

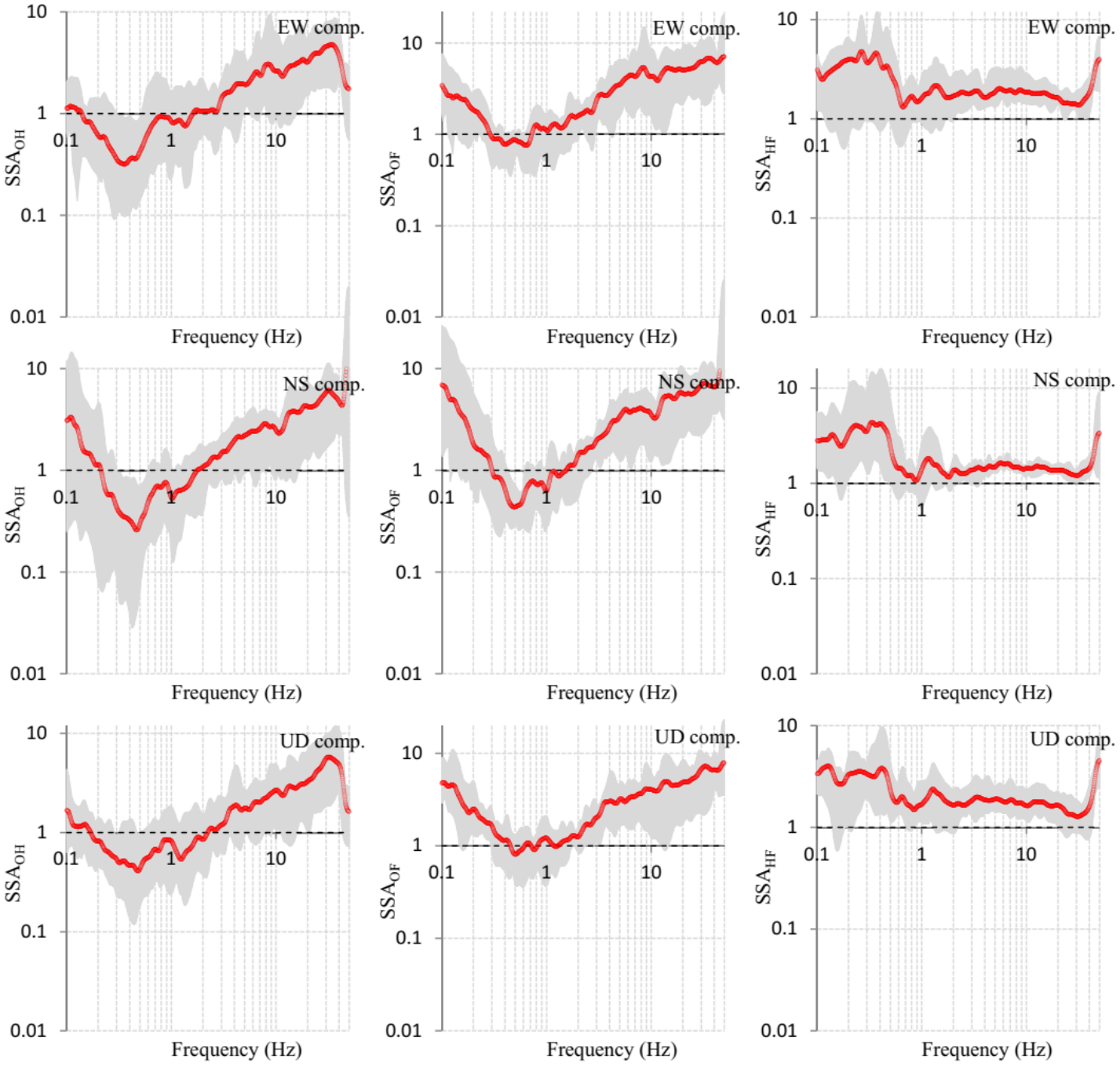

Figure S22: The estimated average SSAs (red) with their minimum and maximum (gray), which are calculated based on equations 1, 2, and 3 for the seismic stations located on the FW block in Fukushima study area.

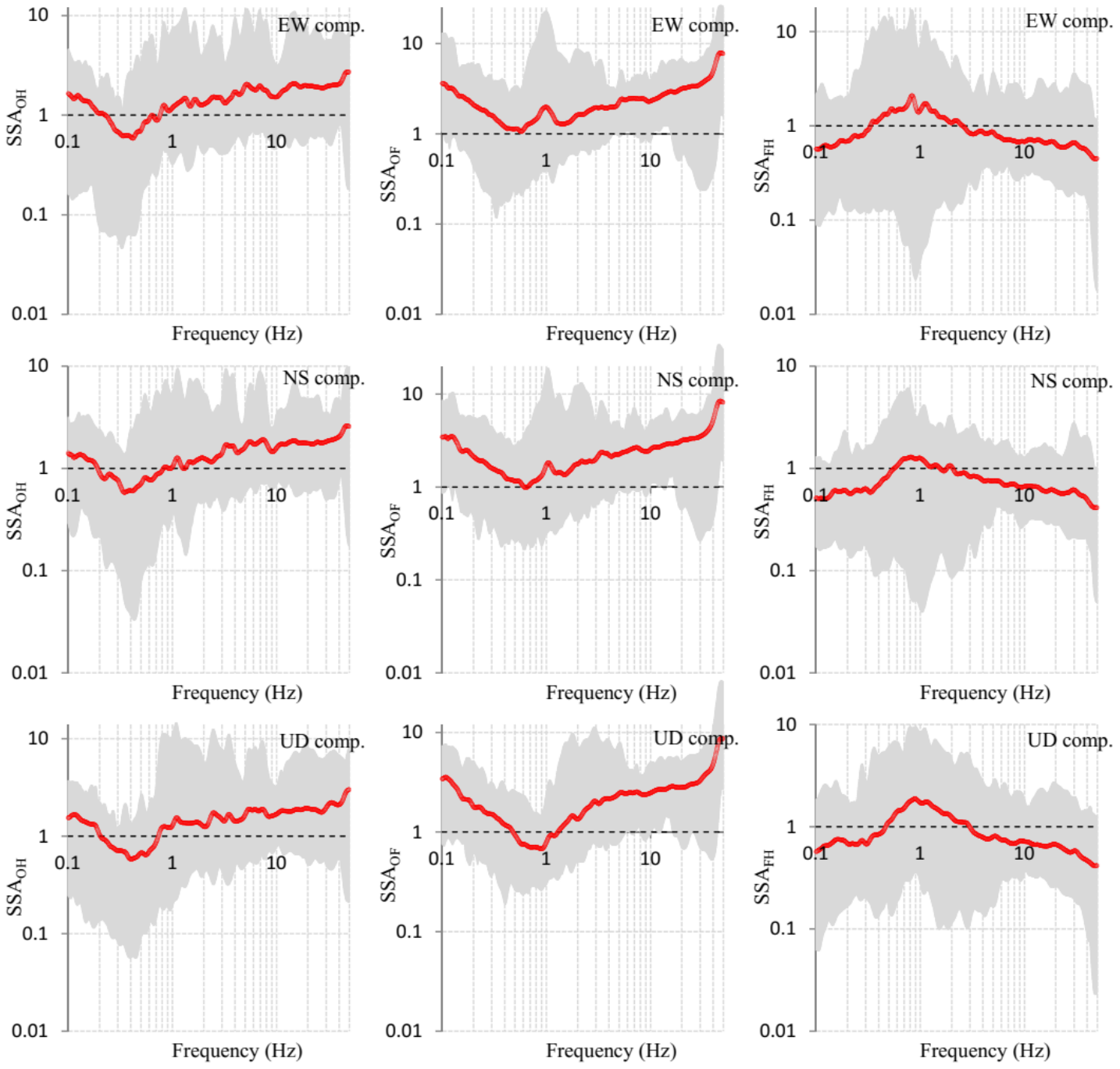

Figure S23: The estimated average SSAs (red) with their minimum and maximum (gray), which are calculated based on equations 1, 2, and 4 for the seismic stations located on the HW block in Fukushima study area.

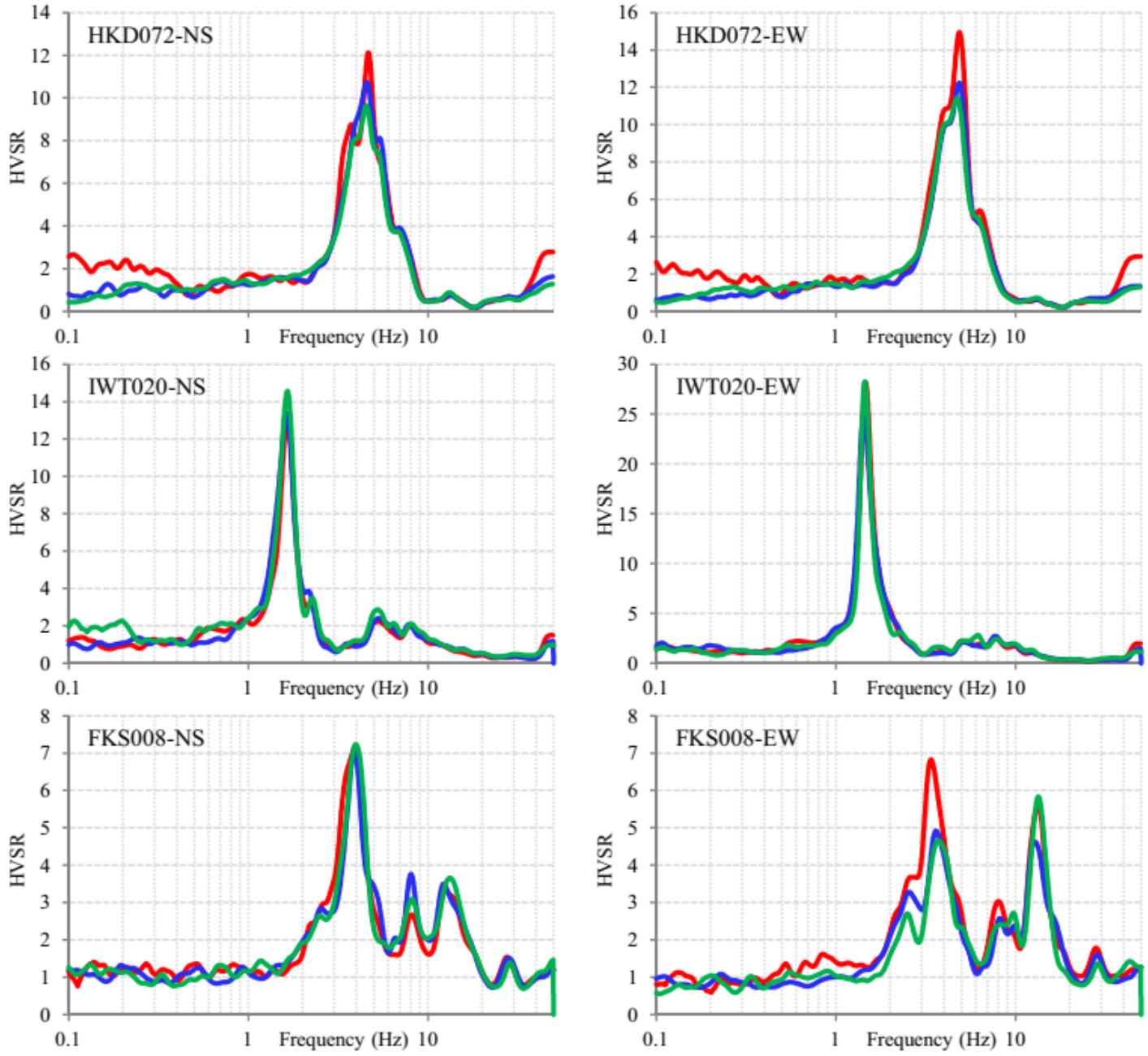

Figure S24: Examples of HVSRs at the three different study areas due to recorded EFWs or Er.FWs in Akita-Iwate area (blue), EFZs (red), EHWs or El.FWs in Akita-Iwate area (green).

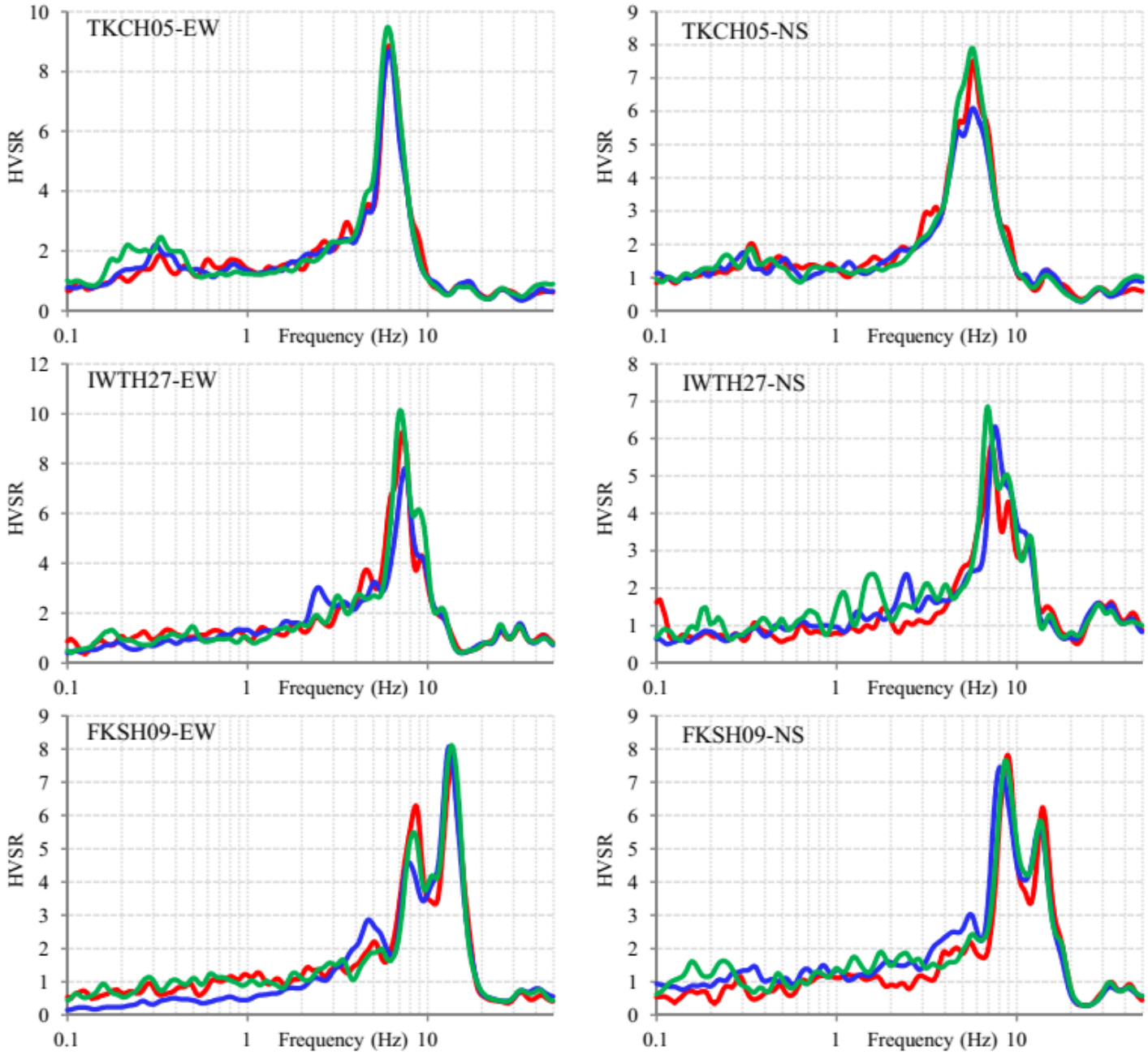

Figure S24: Continued

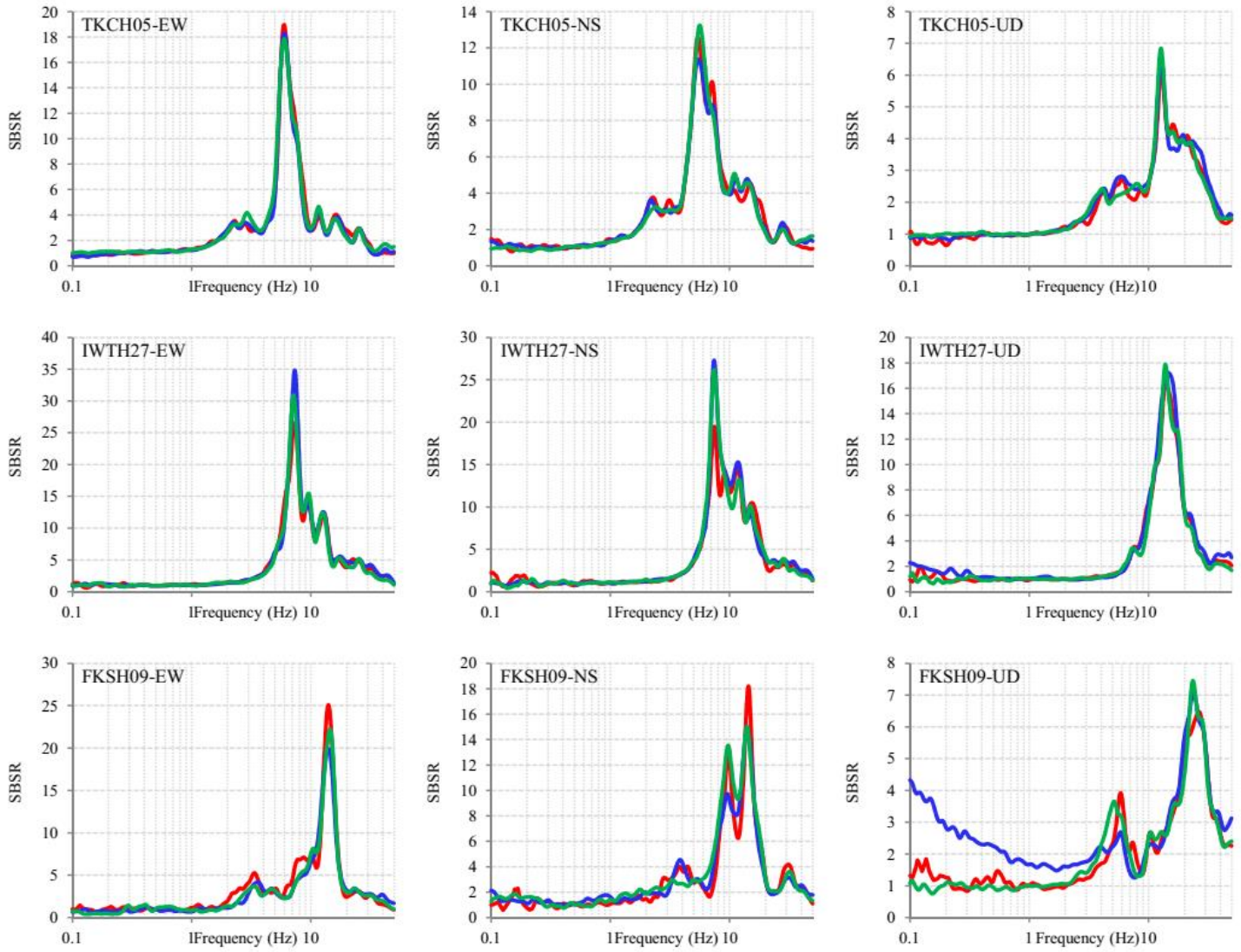

Figure S25: Examples of SBSRs at the three different study areas due to recorded EFWs or Er.FWs in Akita-Iwate area (blue), EFZs (red), EHWs or El.FWs in Akita-Iwate area (green).

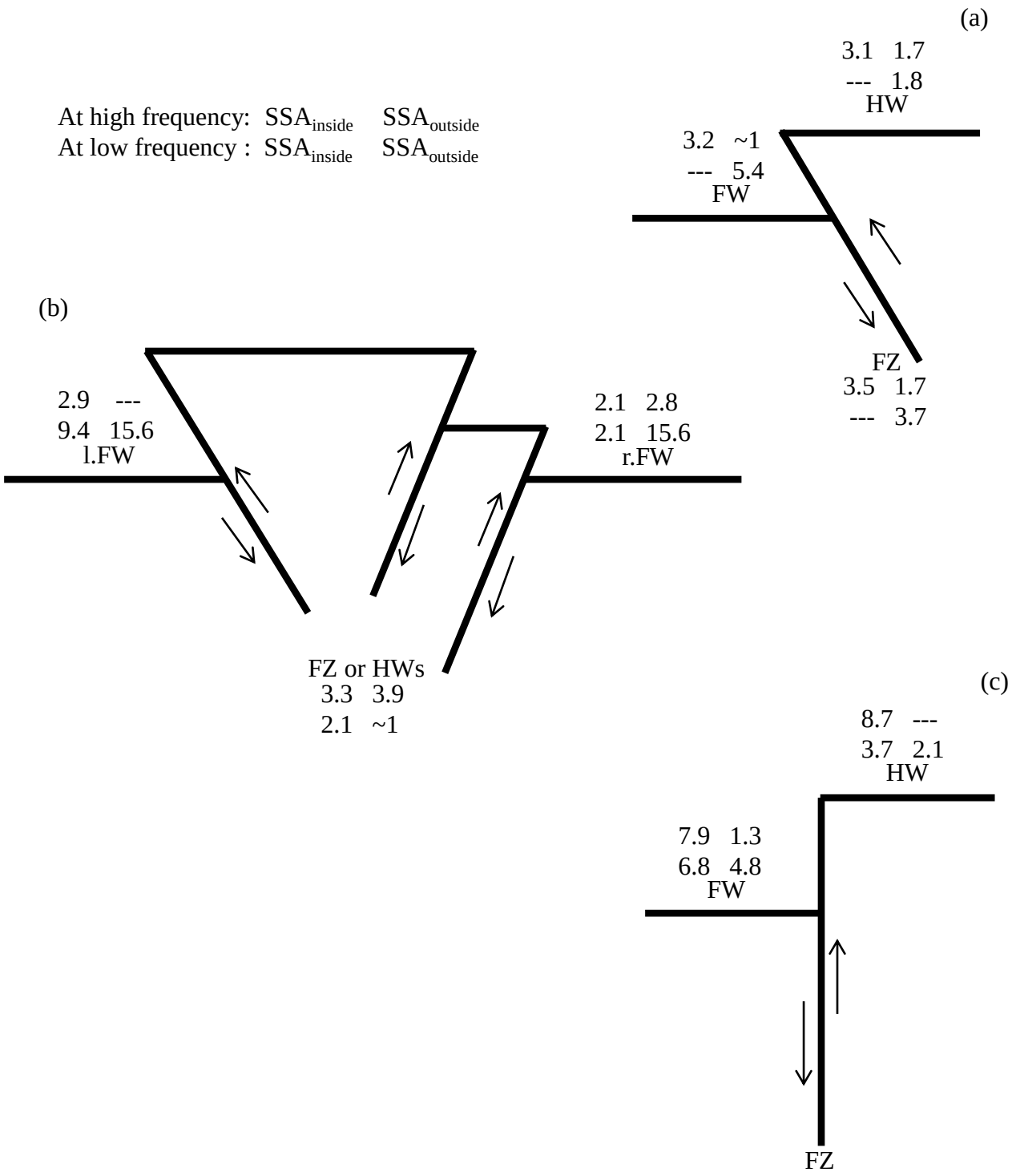

Figure S26: Schematic representations of active fault zones for the three present case studies. (a) East Hokkaido area, (b) Akita-Iwate area, and (c) Fukushima area. (SSA_{inside} and $SSA_{outside}$ are the maximum of averages of SSA (refer to Tables 2, 3, and 4) due to sources inside and outside the active fault zones, respectively.)

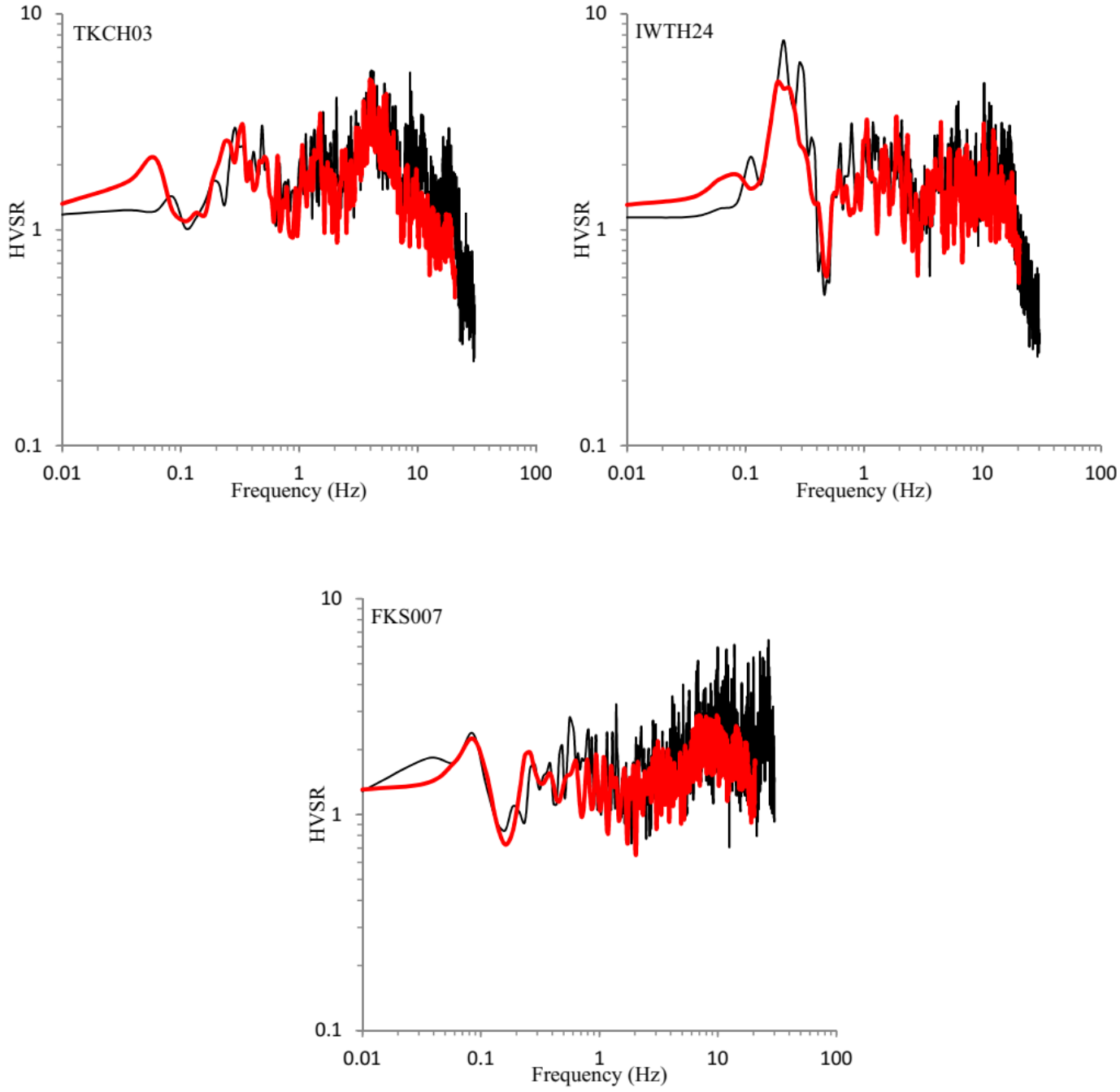

Figure S27: Examples of inverted EHVSRs (red) superimposed with observed HVSRs (black) at three seismic stations on fault zones of the present study.

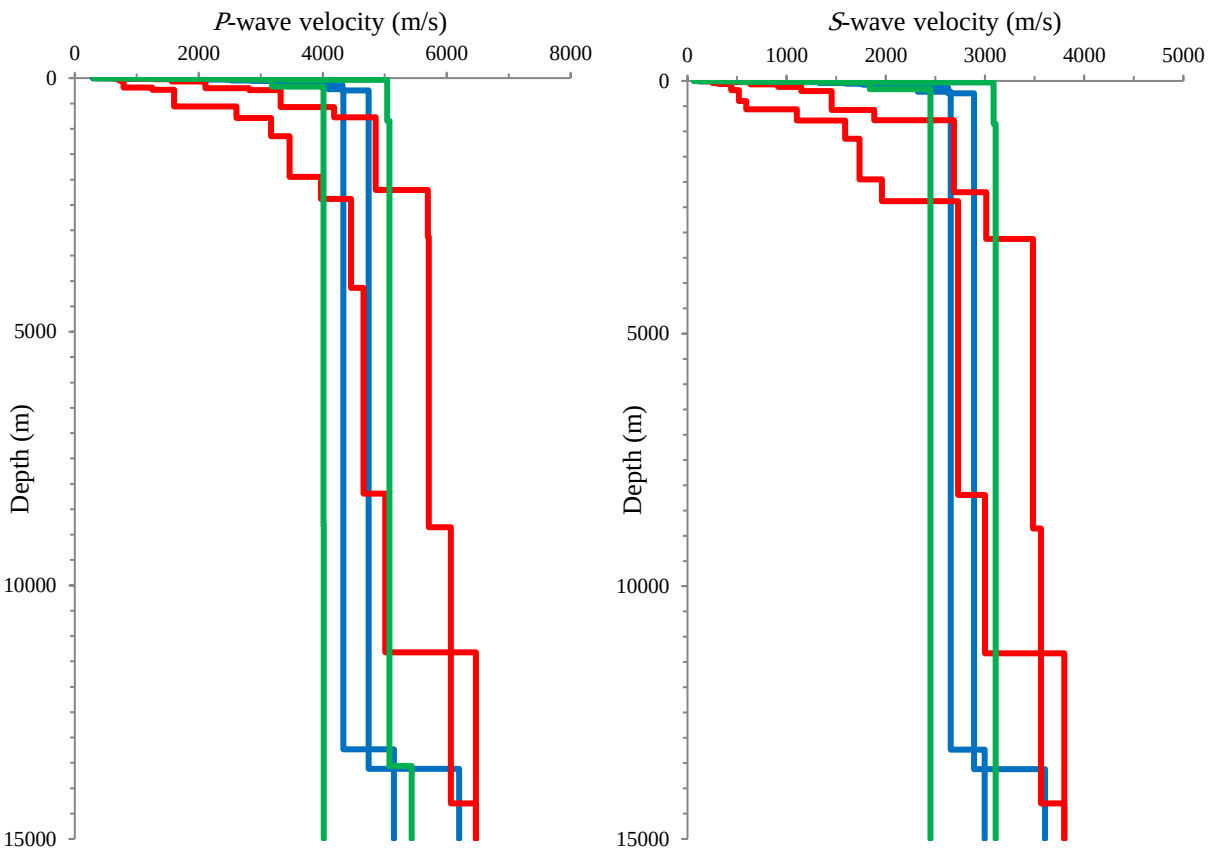

Figure S28: Inverted velocity structures in the Akita-Iwate study area beneath stations on r.FW (blue), FZ (red), and l.FW (green).

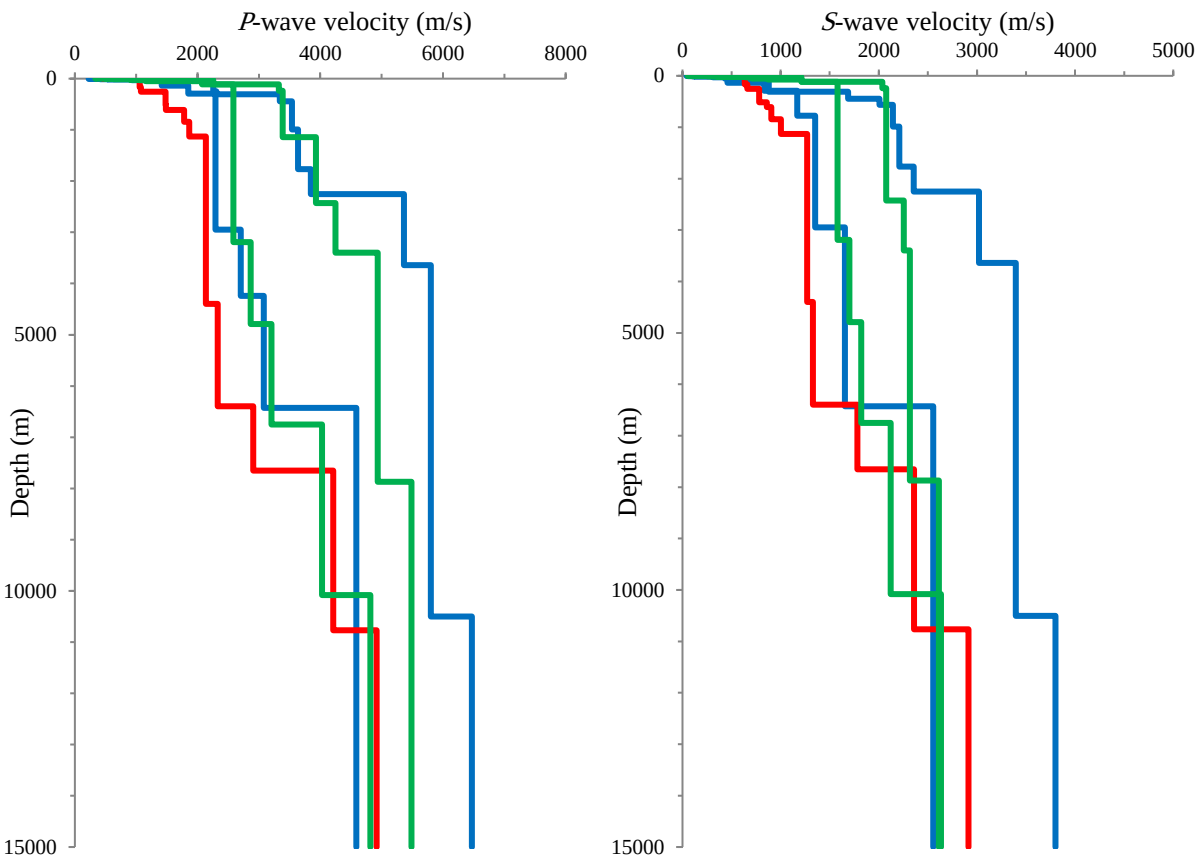

Figure S29: Inverted velocity structures in the Fukushima study area beneath stations on FW (blue), the closest to FZ (red), and HW (green).

Table S1: Characteristics of the behavioral segments of the East Hokkaido active reverse faults (AIST 2013).

Symbol	**a**	**b**	**c**	**d**
Name	Shihoro	Otofuke	Tobetsugawa	Kochien
Description	N-S trending east-dipping reverse fault along the eastern margin of the Tokachi Plain in central Hokkaido	N-S trending east-dipping reverse fault along the eastern margin of the Tokachi Plain in central Hokkaido	N-S trending east-dipping reverse fault along the eastern margin of the Tokachi Plain in central Hokkaido	NW-SE trending northeast-dipping reverse fault along the eastern margin of the Hidaka mountains in central Hokkaido
Trend	10˚	0˚	0˚	330˚
Dip	30˚ E	30˚ E	30˚ E	45˚ E
Length	62 Km	18 Km	40 Km	26 Km
Sense of faulting	Reverse	Reverse	Reverse	Reverse
Upthrown side	East	East	East	East
Slip rate	0.4 m/K years	0.0 m/K years	0.3 m/K years	0.1 m/K years
Slip per Event	7.2 m		4.7 m	3.0 m
Recurrence Interval	18000 years	-----	16000 years	24000 years
Elapsed time rate	-----	-----	-----	0.68
Rupture Probability in next 30 years	0.2 %	-----	0.2 %	0.1 %

Table S2: Characteristics of the behavioral segments of the Akita-Iwate active reverse faults (AIST 2013).

Symbol	**a**	**b**	**c**	**d**	**e**	**f**	**g**	**h**	**i**	**j**
Name	Ukai	Hanamaki	Kitakami-nishi	Shizukuishibonchi-seien	Kawafune	Warikurayama	Tazawako-toho	Senya	Kanazawa	Omoriyama
Description	N-S trending west-dipping reverse fault along the western margin of the Kitakami Basin in northern Honshu	N-S trending west-dipping reverse fault along the western margin of the Kitakami Basin in northern Honshu	N-S trending west-dipping reverse fault along the western margin of the Kitakami Basin in northern Honshu	N-S trending west-dipping reverse fault along the western margin of the Shizukuishi Basin in northern Honshu	NNE-SSW trending west-dipping reverse fault along the eastern margin of the Mahiru Mountains in northern Honshu, ruptured during the 1896 Rikuu earthquake	N-S trending west-dipping reverse fault along the eastern margin of the Mahiru Mountains in northern Honshu	N-S trending east-dipping reverse fault along the eastern shore of Lake Tazawa in northern Honshu, partly ruptured during 1896 Rikuu earthquake	N-S trending east-dipping reverse fault along the eastern margin of the Yokote Basin in northern Honshu, ruptured during the 1896 Rikuu earthquake	N-S trending east-dipping reverse fault along the eastern margin of the Yokote Basin in northern Honshu	N-S trending east-dipping reverse fault along the eastern margin of the Yokote Basin in northern Honshu
Trend	10˚	10˚	350˚	10˚	20˚	0˚	0˚	10˚	0˚	350˚
Dip	45˚ W	45˚ W	45˚ W	45˚ W	45˚ W	45˚ W	45˚ E	30˚E	45˚ E	45˚ E
Length	11 Km	42 Km	27 Km	21 Km	24 Km	17 Km	10 Km	24 Km	17 Km	23 Km
Sense of faulting	Reverse	Reverse	Reverse	Reverse	Reverse	Reverse	Reverse	Reverse	Reverse	Reverse
Upthrown side	West	West	West	West	West	West	East	East	East	East
Slip rate	0.0 m/K years	0.6 m/K years	0.2 m/K years	0.6 m/K years	0.1 m/K years	0.0 m/K years	0.3 m/K years	0.8 m/K years	0.3 m/K years	0.2 m/K years
Slip per Event	-----	4.9 m	3.1 m	2.4 m	2.2 m	-----	1.2 m	2.9 m	2.0 m	2.7 m
Recurrence Interval	-----	8200 years	13000 years	4300 years	22000 years	-----	3900 years	3700 years	6700 years	16000 years
Elapsed time rate	-----	0.51	-----	0.41	0.0	-----	-----	0.03	-----	-----
Rupture Probability in next 30 years	-----	0.4 %	0.2 %	0.7 %	0.1 %	-----	0.8 %	0.8 %	0.5 %	0.2 %

Table S2: Cont.

Symbol	**k**	**l**	**m**	**n**
Name	Takinosawa	Nakacho	Toridame	Kitayuri
Description	N-S trending west-dipping reverse fault in northern Honshu	NNE-SSW trending west-dipping reverse fault in northern Honshu	N-S trending east-dipping reverse fault in northern Honshu	N-S trending east-dipping reverse fault along the western offshore of northern Honshu
Trend	0˚	20˚	0˚	0˚
Dip	45˚ W	45˚ W	45˚ E	45˚ E
Length	18 Km	9 Km	11 Km	29 Km
Sense of faulting	Reverse	Reverse	Reverse	Reverse
Upthrown side	West	West	East	East
Slip rate	0.0 m/K years	0.1 m/K years	0.0 m/K years	0.9 m/K years
Slip per Event	-----	-----	-----	3.4 m
Recurrence Interval	-----	-----	-----	3600 years
Elapsed time rate	-----	-----	-----	0.41
Rupture Probability in next 30 years	-----	-----	-----	0.8 %

Table S3: Characteristics of the behavioral segments of the Fukushima active reverse faults (AIST 2013).

Symbol	**a**	**b**	**c**	**d**
Name	Watari	Haramachi	Namie	Sangunmori
Description	N-S trending west-dipping reverse fault along the eastern margin of the Abukuma Mountains in northern Honshu	N-S trending left-lateral strike-slip fault with west-side-up vertical displacement along the eastern margin of the Abukuma Mountains in northern Honshu	N-S trending west-dipping reverse fault along the eastern margin of the Abukuma Mountains in northern Honshu	N-S trending left-lateral strike-slip fault with east-side-up vertical displacement in the Abukuma Mountains, northern Honshu
Trend	350˚	350˚	350˚	0˚
Dip	80˚ W	90˚ V	80˚ W	90˚ V
Length	21 Km	21 Km	53 Km	15 Km
Sense of faulting	Reverse	L-lateral	Reverse	L-lateral
Upthrown side	West	West	West	East
Slip rate	0.1 m/K years	0.1 m/K years	0.0 m/K years	0.1 m/K years
Slip per Event	2.4 m	1.5 m	-----	1.7 m
Recurrence Interval	24000 years	10000 years	-----	17000 years
Elapsed time rate	-----	0.20	-----	-----
Rupture Probability in next 30 years	0.1 %	0.3 %	-----	0.2 %